plantation of olfactory ensheathing cells in adult rats. *The Journal of Neuroscience*, **23**, 9428-9434.

[28] Ogawa, Y., Sawamoto, K. and Miyata, T. (2002) Transplantation of *in vitro*-expanded fetal neural progenitor cells results in neurogenesis and functional recovery after spinal cord contusion injury in adult rats. *Journal of Neuroscience Research*, **69**, 925-933. doi:10.1002/jnr.10341

[29] Han, S.S., Kang, D.Y. and Mujtaba, T. (2002) Grafted lineage-restricted precursors differentiate exclusively into neurons in the adult spinal cord. *Experimental Neurology*, **177**, 360-375. doi:10.1006/exnr.2002.7995

[30] McDonald, J.W., Liu, X.Z. and Qu, Y. (1999) Transplanted embryonic stem cells survive, differentiate and promote recovery in injured rat spinal cord. *Nature Medicine*, **5**, 1410-1412. doi:10.1006/exnr.2002.7995

[31] Cao, Q.L., Zhang, Y.P. and Howard, R.M. (2001) Pluripotent stem cells engrafted into the normal or lesioned adult rat spinal cord are restricted to a glial lineage. *Experimental Neurology*, **167**, 48-58. doi:10.1006/exnr.2002.7995

[32] Okada, S., Ishii, K. and Yamane, J. (2005) *In vivo* imaging of engrafted neural stem cells: its application in evaluating the optimal timing of transplantation for spinal cord injury. *The FASEB Journal*, **19**, 1839-1841.

[33] Stocum, D.L. (2005) Stem cells in CNS and cardiac regeneration. *Advances in Biochemical Engineering/Biotechnology*, **93**, 135-159. doi:10.1007/b99969

[34] Association ASC (2003) ASIA International Standards for Neurological Classification of Spinal Cord Injury, Revised. Spinal Cord Association.

[35] Pinter, M.M. and Dimitrijevic, M.R. (1999) Gait after spinal cord injury and the central pattern generator for locomotion. *Spinal Cord*, **37**, 531-537. doi:10.1038/sj.sc.3100886

[36] Curt, A., Keck, M.E. and Dietz, V. (1998) Functional outcome following spinal cord injury: Significance of motor-evoked potentials and ASIA scores. *Archives of Physical Medicine and Rehabilitation*, **79**, 81-86. doi:10.1016/S0003-9993(98)90213-1

Transplanted Bone Marrow–Derived Circulating PDGFRα$^+$ Cells Restore Type VII Collagen in Recessive Dystrophic Epidermolysis Bullosa Mouse Skin Graft

Shin Iinuma,*,†,‡,[1] Eriko Aikawa,*,[1] Katsuto Tamai,* Ryo Fujita,† Yasushi Kikuchi,* Takenao Chino,* Junichi Kikuta,§ John A. McGrath,¶ Jouni Uitto,‖ Masaru Ishii,§ Hajime Iizuka,‡ and Yasufumi Kaneda†

Recessive dystrophic epidermolysis bullosa (RDEB) is an intractable genetic blistering skin disease in which the epithelial structure easily separates from the underlying dermis because of genetic loss of functional type VII collagen (Col7) in the cutaneous basement membrane zone. Recent studies have demonstrated that allogeneic bone marrow transplantation (BMT) ameliorates the skin blistering phenotype of RDEB patients by restoring Col7. However, the exact therapeutic mechanism of BMT in RDEB remains unclear. In this study, we investigated the roles of transplanted bone marrow–derived circulating mesenchymal cells in RDEB (Col7-null) mice. In wild-type mice with prior GFP-BMT after lethal irradiation, lineage-negative/GFP-positive (Lin$^-$/GFP$^+$) cells, including platelet-derived growth factor receptor α-positive (PDGFRα$^+$) mesenchymal cells, specifically migrated to skin grafts from RDEB mice and expressed Col7. Vascular endothelial cells and follicular keratinocytes in the deep dermis of the skin grafts expressed SDF-1α, and the bone marrow–derived PDGFRα$^+$ cells expressed CXCR4 on their surface. Systemic administration of the CXCR4 antagonist AMD3100 markedly decreased the migration of bone marrow–derived PDGFRα$^+$ cells into the skin graft, resulting in persistent epidermal detachment with massive necrosis and inflammation in the skin graft of RDEB mice; without AMD3100 administration, Col7 was significantly supplemented to ameliorate the pathogenic blistering phenotype. Collectively, these data suggest that the SDF1α/CXCR4 signaling axis induces transplanted bone marrow–derived circulating PDGFRα$^+$ mesenchymal cells to migrate and supply functional Col7 to regenerate RDEB skin. *The Journal of Immunology*, **2015, 194: 1996–2003.**

Recessive dystrophic epidermolysis bullosa (RDEB) is a severe genetic blistering skin disease in which mutations in both alleles of the type VII collagen gene (COL7A1) abrogate functional expression of Col7, which physiologically secures the attachment of epidermis to the underlying dermis in the cutaneous basement membrane zone. Previously, we reported that allogeneic BMT in the circulation of fetal RDEB mice could restore functional Col7 in the cutaneous basement membrane zone after birth, thereby improving the blistering phenotype of the skin and extending survival (1). Furthermore, in a clinical trial, allogeneic BMT in human RDEB patients ameliorated their fragile skin condition by enhancing Col7 expression (2). However, the exact mechanism underlying the BMT-mediated Col7 supplementation in RDEB skin is still unknown.

Bone marrow contains at least two different lineages of cells: hematopoietic and mesenchymal cells. Hematopoietic cells are generated from hematopoietic stem cells (HSCs), which reside in the bone marrow stem cell niche. Mesenchymal cells are thought to be derived from mesenchymal stem cells (MSCs) in the bone marrow, although the definitive nature of MSCs is still under investigation (3, 4). MSCs were originally defined as stem cells that could differentiate into mesenchymal lineages, such as osteocytes, chondrocytes, and adipocytes, in culture (5–8). However, MSCs were also shown to differentiate into other lineages, including neuronal and epithelial cells (9, 10).

In the field of skin regeneration, bone marrow has been shown to provide inflammatory and noninflammatory cells, including mesenchymal fibroblasts and epidermal keratinocytes, to wounded areas (11–13). We previously reported that bone marrow–derived platelet-derived growth factor receptor α (PDGFRα)-positive mesenchymal cells play a crucial role in regenerating the engrafted skin of wild-type mice and RDEB mice by providing bone marrow–derived fibroblasts and keratinocytes (14). Although

*Department of Stem Cell Therapy Science, Graduate School of Medicine, Osaka University, Suita 565-0871, Japan; †Division of Gene Therapy Science, Graduate School of Medicine, Osaka University, Suita 565-0871, Japan; ‡Department of Dermatology, Asahikawa Medical College, Asahikawa 078-8510, Japan; §Immunology and Cell Biology, Graduate School of Medicine, Osaka University, Suita 565-0871, Japan; ¶Department of Molecular Dermatology, King's College, London WC2R 2LS, United Kingdom; and ‖Department of Dermatology and Cutaneous Biology, Sidney Kimmel Medical College at Thomas Jefferson University, Philadelphia, PA 19107

[1]S.I. and E.A. contributed equally to this work.

Received for publication April 10, 2014. Accepted for publication December 12, 2014.

This work was supported by a Grant-in-Aid for Scientific Research from the Ministry of Education, Culture, Sports, Science, and Technology of Japan and a Health and Labour Sciences Research Grant (for Research of Intractable Diseases and for Clinical Trial on Development of New Drugs and Medical Devices in 2014) from the Ministry of Health, Labour, and Welfare of Japan.

S.I., E.A., and R.F. designed the research, performed the research, and analyzed the data. T.C., Y.K., J.A.M., and H.I. analyzed the data. S.I., E.A., R.F. and K.T. wrote the manuscript. Y.K., J.U., J.K., and M.I. contributed vital reagents. K.T. and Y.K. were responsible for the final approval of the manuscript.

Address correspondence and reprint requests to Prof. Katsuto Tamai, Department of Stem Cell Therapy Science, Graduate School of Medicine, Osaka University, 2-2, Yamada-oka, Suita, Osaka 565-0871, Japan. E-mail address: tamai@gts.med.osaka-u.ac.jp

Abbreviations used in this article: BMT, bone marrow transplantation; HMGB1, high mobility group box 1; HSC, hematopoietic stem cell; MSC, mesenchymal stem cell; PDGFRα, platelet-derived growth factor receptor α; RDEB, recessive dystrophic epidermolysis bullosa; SDF-1α, stromal cell–derived factor 1α.

www.jimmunol.org/cgi/doi/10.4049/jimmunol.1400914

PDGFRα is known to be expressed by cutaneous mesenchymal cells such as dermal fibroblasts and follicular papilla cells, the appearance of PDGFRα$^+$ bone marrow cell-derived keratinocytes is consistent with previous reports that the PDGFRα$^+$ cell population in bone marrow contains ectodermally derived MSCs with neural and epithelial differentiation capacity (15, 16).

Regarding the homing of marrow-derived nonhematopoietic cells into the area in need of repair, previous studies demonstrated that various stimuli derived from injured tissues mobilize MSCs from the bone marrow to accelerate tissue repair (17, 18); however, circulating MSCs are relatively rare under physiologic conditions (19, 20). We also previously demonstrated that necrotic skin, including detached RDEB epithelia, releases high mobility group box 1 (HMGB1), which then mobilizes PDGFRα$^+$ bone marrow cells into the circulation. However, the mechanisms by which bone marrow–derived mesenchymal cells home to injured skin and the role of these cells in RDEB skin after BMT have not been elucidated.

Among chemokines and their receptors, the C-X-C type chemokine ligand 12 (CXCL12), known as stromal cell-derived factor 1α (SDF-1α), and its receptor, CXCR4, have been documented to direct the migration of stem/progenitor cells to various tissues (21–25). In bone marrow, endothelial cells and stromal cells in the HSC niche express SDF-1α, which acts as a chemoattractant for HSCs and supports the survival and proliferation of HSCs via CXCR4 signaling (25, 26). SDF-1α is also implicated in the migration of circulating CXCR4$^+$ stem/progenitor cells to damaged tissues (21–24). The SDF-1α–dependent homing mechanism of circulating endothelial progenitor cells to infarcted myocardium is well established (23, 24). We also previously reported that circulating osteoblast progenitor cells migrate to bone-forming sites via SDF-1α–mediated chemoattraction (22). Furthermore, it has been reported that culture-expanded MSCs are recruited to bone fracture sites by the SDF-1α/CXCR4 pathway after systemic injection (21). SDF-1α expression is regulated by the transcription factor hypoxia inducible factor-1 in endothelial cells in ischemic tissue, thus enabling CXCR4$^+$ stem/progenitor cells in the circulation to target ischemic or injured tissue (23). Although these reports clearly illustrate the SDF-1α/CXCR4 axis as a pivotal mechanism for recruiting various types of bone marrow–derived cells to injured tissues, the roles and functions of these cells in tissue regeneration have not been fully elucidated.

In this study, we examined the role of migrating, bone marrow-derived PDGFRα$^+$ cells in restoring Col7 in RDEB mouse skin engrafted onto GFP-BMT mice. We then investigated the involvement of the SDF-1α/CXCR4 axis in the migration of circulating bone marrow–derived PDGFRα$^+$ cells into the engrafted mouse skin to ameliorate the RDEB phenotype.

Materials and Methods

Mice

All animal experiments were performed according to the guidelines of the Ethical Committee for Animal Experiments of Osaka University Graduate School of Medicine. All experimental mice were housed in cages with a 12-h light-dark cycle. Solid food and water were supplied ad libitum. C57BL/6N mice were purchased from CLEA Japan (Tokyo, Japan). Type VII collagen (Col7) heterozygous ($^{+/-}$) mice were crossed to breed Col7-null ($^{-/-}$) mice, which phenotypically mimic several conditions, including extensive cutaneous blistering suggestive of the human RDEB phenotype (27). C57BL/6N mice that ubiquitously expressed enhanced GFP (GFP, referred to as GFP mice) were provided by Masaru Okabe (Osaka University). SDF-1α/GFP knock-in mice, in which the *GFP* gene was inserted into the SDF-1α locus, were provided by Masaru Ishii (Osaka University).

Bone marrow transplantation

Bone marrow cells were isolated from 6-wk-old male GFP mice by flushing the tibiae and femurs. The recipients were 6-wk-old female C57BL/6N mice that were lethally irradiated with 10 Gy of X-rays, and each irradiated recipient received 5×10^6 bone marrow cells from GFP mice. Experiments were performed on the BMT mice at least 6 wk after BMT.

Skin graft model

Full-thickness skin from wild-type and Col7-null newborn mice (2 × 2 cm) was carefully isolated by excision after the mice had been euthanized under systemic anesthesia and engrafted on the backs of GFP-BMT mice and wild-type mice just above the muscular fascia. The wound sites on the skin-grafted mice were then covered with bandaging tape to protect the grafted skin from scratching until further examination.

ELISA for SDF-1α

Peripheral blood was taken from the heart using a 22-gauge needle and a 1-ml syringe containing heparin. For the preparation of serum, whole blood was centrifuged at 1200 × *g* for 15 min at 4°C. The serum SDF-1α level in each sample was quantitatively analyzed using an SDF-1α ELISA kit; R&D Systems, Minneapolis, MN) according to the manufacturer's instructions.

Immunofluorescent microscopy

The grafted skin pieces were harvested and subjected to immunofluorescent analysis. The excised skin pieces were soaked overnight in 4% paraformaldehyde, embedded in Tissue-Tec OCT Compound (Sakura Finetek, Torrance, CA), frozen on dry ice, and stored at −80°C. For immunofluorescent staining, 7-μm-thick sections were incubated with goat polyclonal anti-mouse Col7 Ab (generated in our laboratory), goat polyclonal anti-mouse PDGFRα Ab (1:200; R&D Systems), rat monoclonal anti-mouse CD31 Ab (1:50; BD Pharmingen, San Diego, CA), rabbit monoclonal anti-mouse cytokeratin 5 (K5) Ab (1:500; Abcam), rat monoclonal anti-mouse neutrophil marker Ab (1:200; Santa Cruz Biotechnology, Dallas, TX), and rat monoclonal anti-mouse CD68 Ab (1:200; Abcam, Cambridge, MA) followed by Alexa Fluor 546-conjugated donkey anti-goat IgG, Alexa Fluor 488-conjugated goat anti-rabbit IgG, and Alexa Fluor 546-conjugated goat anti-rat IgG (1:400; Molecular Probes) as the secondary Abs. The sections were then stained with DAPI and mounted with VECTA Shield anti-fade solution (Vector Laboratories). All images were obtained using a Nikon model A1/C1 confocal laser microscope using NIS-Elements AR 3.1 software (Nikon).

Flow cytometry and cell sorting

The grafted skin was harvested and cut into small pieces using scissors. Tissue pieces were dissociated enzymatically in DMEM (Nacalai Tesque, Kyoto, Japan) containing 0.2% collagenase A (Roche Diagnostics, Tokyo, Japan) at 37°C for 1 h with gentle agitation. The obtained cell suspensions were filtered through a cell strainer. Bone marrow cells were isolated as described above. The fluorescence-conjugated Abs used in this study were as follows: APC anti-mouse lineage mixture with isotype control (BD Pharmingen), PE anti-mouse PDGFRα Ab (eBioscience, San Diego, CA), APC anti-mouse PDGFRα Ab (eBioscience), PE anti-mouse CXCR4 Ab (BD Biosciences), and Alexa Fluor 647-conjugated anti-mouse CXCR4 Ab (BioLegend, San Diego, CA). The stained cells were analyzed using a FACSCanto II device (BD Biosciences) and FlowJo 7.6.1 software (Tree Star, Portland, OR).

For the cell sorting experiments, a BD FACSAria II device (BD Biosciences) was used. Sorting gates were defined based on isotype control staining. RNA from the sorted cells was obtained using Isogen (Nippon Gene, Toyama, Japan) according to the manufacturer's instructions and then subjected to conventional RT-PCR.

Real-time PCR

The engrafted skin was harvested and subjected to real-time PCR analysis. Total RNA was prepared using an RNeasy RNA isolation kit (Qiagen, Hilden, Germany) according to the manufacturer's protocol. cDNA was synthesized using the High-Capacity cDNA Reverse Transcription Kit (Applied Biosystems, Foster City, CA). mRNA was quantified by real-time PCR using SYBR Premix Ex Taq (Takara Bio, Otsu, Shiga, Japan). Real-time PCR was performed and analyzed using the ABI Prism 7900HT Sequence Detection System (Applied Biosystems) and the following primer sets: PDGFRα: 5′-GACGAGTGTCCTTCGCCAAAGTG-3′ (forward) and 5′-CAAAATCCGACCAAGCACGAGG-3′ (reverse); CD11b: 5′-CAATAGCCAGCCTCAGTGC-3′ (forward) and 5′-GAGCCCAGGGGAGAAGTG-3′ (reverse); F4/80: 5′-AAGCATCCGAGACACACACA-3′ (forward) and 5′-GGCAAGACATACCAGGGAGA-3′ (reverse); glyceraldehyde 3-phosphate dehydrogenase (GAPDH): 5′-ACTCCCACTCTTCCACCTTC-3′ (forward) and 5′-TCTTGCTCAGTGTCCTTGC-3′ (reverse);

SDF-1α: 5′-CTGTGCCCTTCAGATTGTTG-3′ (forward) and 5′-TAATTTCGGGTCAATGCACA-3′ (reverse); TATA box binding protein (TBP): 5′-ACGGACAACTGCGTTGATTT-3′ (forward) and 5′-TTCTTGCTGCTAGTCTGGATTG-3′ (reverse). Col7a1 was detected using commercially designed primers (Qiagen). The expression level of SDF-1α was normalized to TBP.

Delivery of CXCR4 antagonist

To ensure sufficient levels of the antagonist throughout the experimental period, we used osmotic Alzet (Alza Corporation, Vacaville, CA) pumps to deliver the CXCR4 antagonist AMD3100 (Sigma-Aldrich, St. Louis, MO) at a constant rate of 10 mg/kg/day. The Alzet pumps were loaded with AMD3100 or PBS and implanted s.c. 1 h before skin graft.

Statistical analysis

Statistical analyses were performed using JMP 8 software. The results are presented as the mean ± SEM. Statistical significance was evaluated using unpaired Student t tests for comparisons between two groups or using ANOVAs for multiple comparisons; $p < 0.05$ was considered statistically significant.

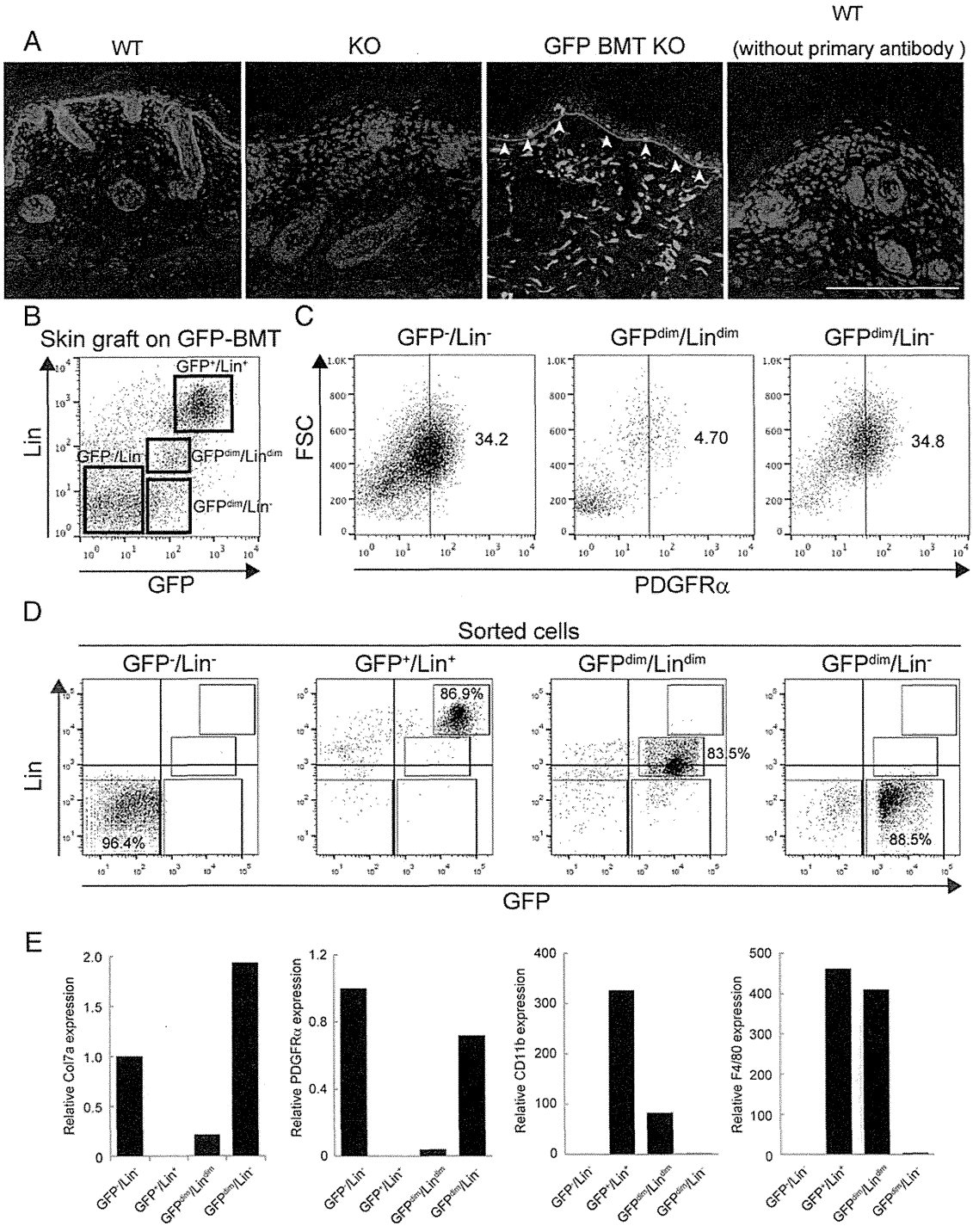

FIGURE 1. Col7 supplementation by bone marrow–derived nonhematopoietic cells. (**A**) Immunostaining of a Col7-null mouse skin graft on a GFP-BMT mouse at day 28. Red, Col7; green, GFP; Blue, DAPI. Scale bar, 50 μm. Arrowheads point to the basement membrane zone. (**B**) Flow cytometric analysis of cells in Col7-null mouse skin grafts on GFP-BMT mice at day 28. (**C**) Flow cytometric analysis of PDGFRα expression in cells from Col7-null skin grafts. (**D**) FACS cell profiles. (**E**) Gene expression of Col7, PDGFRα, CD11b, and F4/80 in sorted cells. GAPDH was used as an internal control.

Results

Transplanted bone marrow–derived non-hematopoietic cells, including PDGFRα$^+$ mesenchymal cells, provide Col7 to RDEB mouse skin grafts

We first examined the particular cell populations that produce Col7 in RDEB mouse skin engrafted onto wild-type mice treated with GFP-BMT after a lethal dose of radiation. Increased numbers of GFP$^+$ bone marrow–derived cells migrated to the RDEB mouse skin grafts, resulting in a restoration of Col7 at the basement membrane zone by day 28 after skin grafting (Fig. 1A). To determine the particular population of bone marrow–derived cells supplying Col7 to the engrafted RDEB mouse skin, we performed flow cytometric analysis of Col7-null skin grafts and identified four populations: GFP$^-$/Lin$^-$ cells, GFP$^+$/Lin$^+$ cells, GFP^{dim}/Lin^{dim} cells, and GFP^{dim}/Lin$^-$ cells (Fig. 1B). In addition, flow cytometry also showed that PDGFRα was predominantly expressed by GFP^{dim}/Lin$^-$ cells, suggesting that this population includes bone marrow–derived MSCs (Fig. 1C). The GFP$^-$/Lin$^-$ cell population, which likely includes resident skin keratinocytes and fibroblasts, also expressed PDGFRα. Then, the four populations of the Col7-null skin grafts were separated using FACS (Fig. 1D), and the gene expression profile of each population (GFP$^-$/Lin$^-$ cells, GFP$^+$/Lin$^+$ cells, GFP^{dim}/Lin^{dim} cells, and GFP^{dim}/Lin$^-$ cells) was analyzed (Fig. 1E). Real-time PCR analysis indicated that GFP^{dim}/Lin$^-$ cells highly expressed Col7a1 in Col7-null skin grafts. However, GFP$^-$/Lin$^-$ cells also expressed Col7a1, suggesting that resident cells from the intact skin adjacent to the skin graft migrated to the Col7-null skin graft and produced Col7a1. The expression levels of Col7a1 and PDGFRα were barely detectable in GFP$^+$/Lin$^+$ cells and GFP^{dim}/Lin^{dim} cells. Instead, GFP$^+$/Lin$^+$ cells and GFP^{dim}/Lin^{dim} cells highly expressed CD11b, a marker for macrophages, NK cells, and granulocytes, as well as F4/80, a marker for pan-macrophages (Fig. 1E). These results suggest that GFP$^+$/Lin$^+$ cells and GFP^{dim}/Lin^{dim} cells include hematopoietic lineage cell populations, such as monocytes and macrophages. Taken together, these data suggest that Col7a1 was primarily supplied by bone marrow–derived nonhematopoietic cells, including the PDGFRα$^+$ MSC population (GFP^{dim}/Lin$^-$). Because mouse MSCs express Col7 in culture (28), we next focused on the mechanism of bone marrow–derived PDGFRα$^+$ cell migration to the grafted skin.

Specific accumulation of bone marrow–derived PDGFRα$^+$ cells in grafted skin

We then examined the accumulation of bone marrow–derived GFP$^+$/PDGFRα$^+$ cells in the wild-type skin grafted on the backs of GFP-BMT mice using immunofluorescent analysis. Because dermal fibroblasts also express PDGFRα, many GFP$^-$/PDGFRα$^+$ cells were observed in the dermis of the graft. Among these cells, GFP$^+$/PDGFRα$^+$ cells were disseminated over the entire dermis of the skin graft, indicating that bone marrow–derived PDGFRα$^+$ cells migrated into the skin graft (Fig. 2A).

To analyze the GFP$^+$/PDGFRα$^+$ cells quantitatively in the skin graft, the day 1, day 4, and day 7 grafts were harvested, and single-cell suspensions of these skin grafts were then subjected to flow cytometric analysis. The quantitative analysis indicated a gradual and significant elevation of the GFP$^+$/PDGFRα$^+$ cell population in the skin graft, reaching over 1.0% of all cells in the day 7 graft (Fig. 2B, 2C). Nongrafted areas in the skin of the same mice did not show such an increase (Fig. 2C), which strongly suggests the existence of a specific recruiting mechanism in the grafted skin. It should be noted, however, that bone marrow PDGFRα$^+$ cells had already significantly migrated into the nongrafted skin of the mice at day 0 (Fig. 2C), albeit at lower levels than in the grafted skin. This migration was possibly the result of a different recruiting mechanism induced by lethal dose irradiation-induced cutaneous injury or another intrinsic mechanism of the skin.

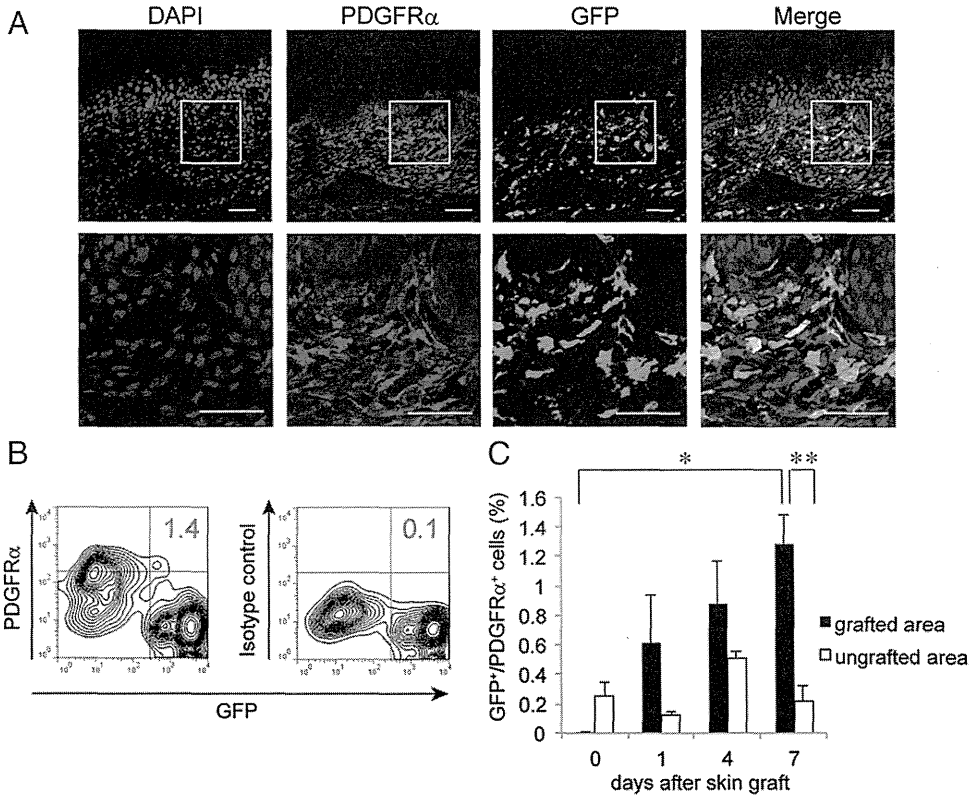

FIGURE 2. Recruitment of bone marrow–derived PDGFRα$^+$ cells into grafted skin. (**A**) Immunostaining of grafted skin on a GFP-BMT mouse at day 7. A portion of bone marrow-derived cells (GFP$^+$) stained positively for PDGFRα in the dermis. Green, GFP; red, PDGFRα; blue, DAPI. Scale bars, 50 μm. The boxed region is displayed in lower panels at a higher magnification. (**B**) Flow cytometric analysis of cells obtained from grafted skin on GFP-BMT mice at day 4. GFP and PDGFRα double-positive cells were detected in grafted skin. (**C**) Time course analysis of GFP$^+$/PDGFRα$^+$ cell migration in grafted skin and nongrafted skin. (n = 4 per group) Values are the mean ± SEM. *p < 0.05, **p < 0.01.

Endothelial and follicular cells are sources of SDF-1α in grafted skin

To determine whether the SDF-1α/CXCR4 axis plays a specific role in recruiting bone marrow–derived circulating PDGFRα+ cells into the grafted skin, we then compared SDF-1α expression in the grafted and non-grafted areas of the skin. Real-time PCR analysis revealed that SDF-1α expression was significantly increased in the skin graft after transplantation, and the maximal increase was observed in the day 4 graft (Fig. 3A). By contrast, no such increase was observed in the non-grafted area (Fig. 3A). These data suggest a critical role of SDF-1α in the graft-specific recruiting mechanism. However, the serum SDF-1α level did not increase after skin grafting (Fig. 3B), which suggests a regional rather than a systemic role of SDF-1α in recruitment.

To determine the particular cell population in the skin graft releasing SDF-1α, we examined SDF-1α expression in skin grafted from a SDF-1α/GFP knock-in mouse onto wild-type mice

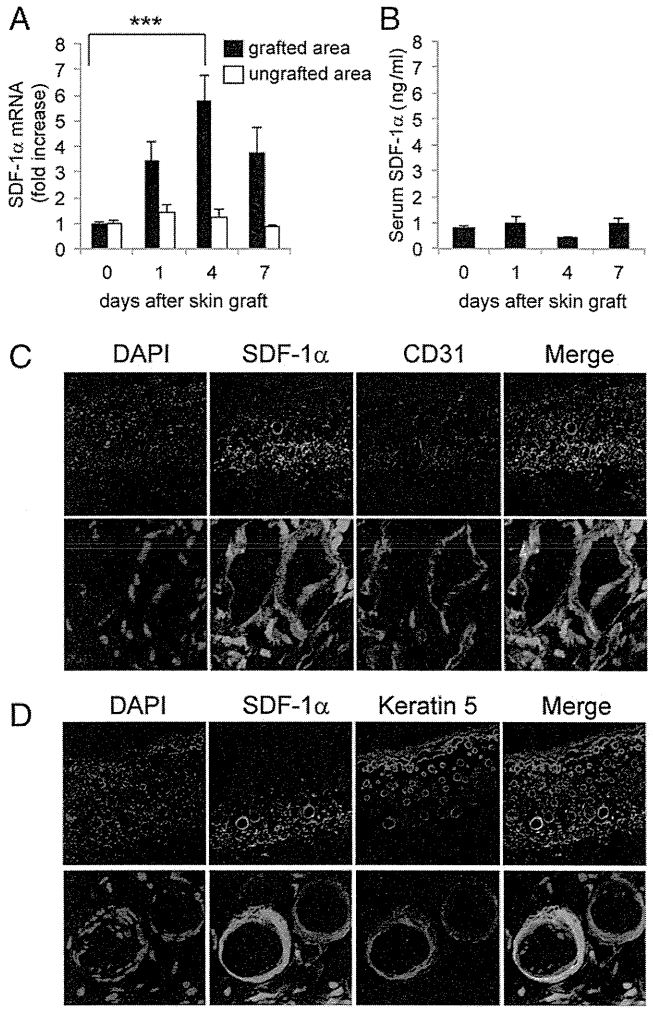

FIGURE 3. SDF-1α expression in grafted skin. (**A**) SDF-1α mRNA expression normalized by TBP (internal control) was determined using real-time PCR at the indicated time points in grafted skin and nongrafted skin. Data are expressed as the fold increase versus the nontreated control (day 0). Values are the mean ± SEM. $n = 4$ per group. ***$p < 0.001$. (**B**) SDF-1α levels in the serum were determined using ELISA at the indicated time points after skin grafting. (**C** and **D**) Immunostaining with CD31 (C) or keratin 5 (K5) (D) of a day 4 skin graft of a SDF-1α/GFP knock-in mouse. SDF-1α was colocalized with both CD31 and K5 in the deep dermis of the grafted skin. Lower panels show the colocalized regions at higher magnification. Green, SDF-1α; red, CD31, K5; blue, DAPI. Scale bars, 100 μm. $n = 4$ per group.

at day 4. The SDF-1α/GFP signal was detected in the deep dermal cells of the graft (Fig. 3C). A previous report indicated that endothelial cells are major sources of SDF-1α in the dermis of hypoxic skin flaps (23). We therefore stained the day 4 graft samples with the endothelial cell marker CD31 and the keratinocyte marker cytokeratin 5 (K5). As expected, CD31+ cells in the deep dermis of the graft were costained with SDF-1α/GFP (Fig. 3C, 3D), which indicates that CD31+ endothelial cells in the deep dermis were the sources of SDF-1α in the grafted skin. It is particularly interesting that follicular keratinocytes expressing K5 in the deep dermis, and not epidermal cells, also showed significant SDF-1α expression. Because cultured epidermal keratinocytes and separated epidermal sheets from the skin grafts did not show SDF-1α expression via real-time PCR (data not shown), a follicular keratinocyte-specific recruiting mechanism for CXCR4+ cells is suggested.

The SDF-1α/CXCR4 axis is essential for recruiting bone marrow–derived PDGFRα+ cells to grafted skin

To confirm that the SDF-1α/CXCR4 axis plays an essential role in the specific recruitment of bone marrow–derived PDGFRα+ cells to the grafted skin, we then analyzed the expression of CXCR4 on PDGFRα+ cells in both the bone marrow and the day 4 grafts. In freshly isolated mouse bone marrow cells, expression of CXCR4 was detected on PDGFRα+ cells via flow cytometry (Fig. 4A). CXCR4 expression was also observed on the surface of GFP+/PDGFRα+ cells from day 4 grafts on GFP-BMT mice (Fig. 4B). To assess the role of CXCR4 in recruiting PDGFRα+ cells to the skin grafts, we systemically administered the CXCR4 antagonist AMD3100 using an osmotic pump implanted s.c. into GFP-BMT mice prior to skin grafting. A drastic reduction of GFP+/PDGFRα+ cell migration was observed in skin grafts on the mice systemically administered with AMD3100, but not with PBS (Fig. 4C, 4D). These data demonstrate a critical role of the SDF-1α/CXCR4 axis in the specific recruitment of PDGFRα+ bone marrow cells to grafted skin.

PDGFRα+ cells play a pivotal role in the regeneration of RDEB mouse skin grafts

We examined the effects of blocking PDGFRα+ cell migration on the regeneration of RDEB mouse skin grafts. Without AMD3100 administration, linear deposition of Col7 along the dermal–epidermal junction was clearly restored throughout day 14 graft of RDEB mouse skin (Fig. 5A). As a result, a regenerated epidermis was maintained without significant blistering in the day 14 graft (Fig. 5B). By contrast, with systemic AMD3100 administration, Col7 restoration was almost completely interrupted at the dermal–epidermal junction of the Col7-null mouse skin graft (Fig. 5A), resulting in separation and degeneration of the epidermis with massive inflammatory cell infiltration in the dermis (Fig. 5B). These data suggest that the SDF-1α/CXCR4 axis-mediated migration of bone marrow–derived PDGFRα+ cells is essential for restoring Col7 in the cutaneous basement membrane zone of Col7-null mouse skin grafts.

For further analysis of the increased infiltration of mononuclear cells in AMD3100-treated mice, we performed immunostaining with a neutrophil marker and CD68, which is a cell surface marker for macrophages. There was an increase in neutrophil marker-positive cells in the AMD3100-treated group (Fig. 5C). Furthermore, there was a significant increase in the number of CD68 positive cells in the AMD3100-treated group (Fig. 5D). These data suggest that CXCR4-antagonist treatment of Col7-null skin grafted mice also enhanced inflammation in the skin grafts by increasing the infiltration of neutrophils and macrophages.

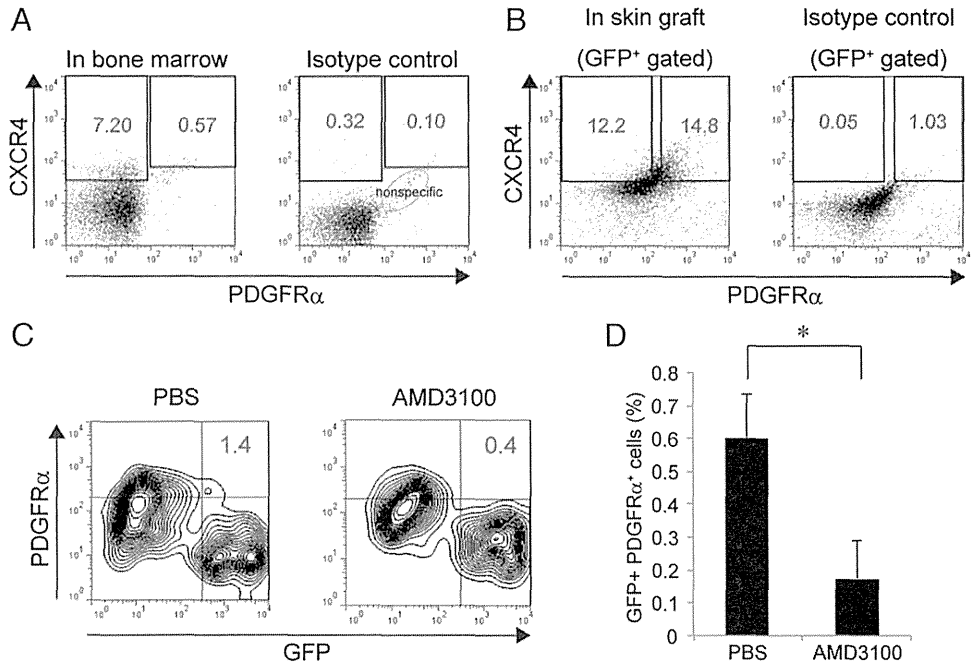

FIGURE 4. Effect of a CXCR4 antagonist on PDGFRα$^+$ cell migration into the grafted skin. (**A**) Flow cytometric analysis of CXCR4 in freshly isolated PDGFRα$^+$ bone marrow cells. Some PDGFRα$^+$ cells in the bone marrow expressed CXCR4. (**B**) Flow cytometric analysis of CXCR4 on GFP$^+$/PDGFRα$^+$ cells that had migrated into skin grafted onto GFP-BMT mice by day 4. CXCR4$^+$/GFP$^+$/PDGFRα$^+$ cells were observed in the grafted skin. (**C**) Flow cytometric analysis of GFP$^+$/PDGFRα$^+$ cells in skin grafted onto GFP-BMT mice at day 4 with or without treatment of the CXCR4 antagonist AMD3100. (**D**) Quantitative analysis of GFP$^+$/PDGFRα$^+$ cells in grafted skin using flow cytometry on day 4 with or without AMD3100 treatment. The migration of GFP$^+$/PDGFRα$^+$ cells into grafted skin was significantly blocked by AMD3100. $n = 4$ per group. Values are the mean ± SEM. $*p < 0.05$.

Discussion

In this study, we provide evidence that transplanted bone marrow-derived nonhematopoietic cells, including PDGFRα$^+$ cells, play a crucial role in regenerating the skin of RDEB mice by restoring Col7 in the cutaneous basement membrane zone following BMT. We also demonstrate an indispensable role of the SDF-1α/CXCR4 axis for recruiting bone marrow–derived PDGFRα$^+$ cells to grafted skin, in which blood circulation is initially terminated, resulting in a severely hypoxic/necrotic condition. These data support the notion of allogeneic BMT as a novel therapeutic option for severely affected RDEB patients who have impaired Col7 expression and numerous necrotic lesions in the skin.

PDGFRα is an established marker for mouse bone marrow MSCs, which include ectodermally derived multipotent stem cells (29). Intravenously transplanted cultured mouse MSCs were previously shown to accumulate in wounded skin and differentiate into multiple skin cell types, including fibroblasts, endothelial cells, pericytes, and keratinocytes (30). Bone marrow–derived PDGFRα$^+$ cells can also differentiate into ectodermal keratinocytes and mesenchymal dermal fibroblasts, particularly in the setting of skin grafts (14). Bone marrow–derived keratinocytes were observed in skin grafts up to 5 mo after transplantation in a previous report, suggesting supplementation of resident epidermal progenitor/stem cells from the bone marrow. In this study, we detected bone marrow–derived mesenchymal cells in the dermis in day 7 skin grafts, suggesting that bone marrow–derived PDGFRα$^+$ cells primarily serve as mesenchymal cells, such as fibroblasts, in the dermis of a skin graft or wound, but have the potential to become keratinocytes in a particular milieu or niche to induce an epigenetic transition from mesenchymal to epithelial lineages, particularly in RDEB skin (14).

In addition to their multidifferentiation potential, MSCs have been shown to promote wound healing processes by providing various trophic factors in lesions. For example, MSCs locally administered into injured tissue promote neovascularization by releasing proangiogenic cytokines, such as vascular endothelial growth factor-α, insulin-like growth factor-1, PDGF-BB, and angiopoietin-1 (31, 32). Recently, transplanted MSCs were shown to suppress immune and inflammatory reactions by releasing anti-inflammatory molecules, including IL-10, PG-E, and TNF-stimulated gene-6 protein (33–36). In the current study, the massive inflammatory reaction observed in the skin grafts when PDGFRα$^+$ cell migration was blocked suggests that these cells also have anti-inflammatory activity. Therefore, the migration of bone marrow–derived PDGFRα$^+$ cells seems to play multiple roles in the regeneration of injured skin and in the engraftment of skin grafts.

Accumulating evidence, including that presented in this study, has defined a crucial role of the SDF-1α/CXCR4 axis in recruiting bone marrow–derived MSCs for the regeneration of tissue in conditions such as bone fractures (21), brain damage (37), and infarcted myocardium (38). However, several reports have provided contradictory results. One report found that MSCs lack many effectors of homing, particularly CXCR4 (39), whereas another study indicated that MSCs use β1 integrin, not CXCR4, for myocardial migration and engraftment (40). This discrepancy may be partially explained by the amount or duration of SDF-1α expression in damaged tissue. In this context, augmentation of the SDF-1α/CXCR4 axis by overexpression, drug treatment, or both may enhance further recruitment of MSCs to various types of tissue damage. This concept could be a promising therapeutic strategy for the effective delivery of MSCs.

We demonstrate in this study that transplanted bone marrow–derived PDGFRα$^+$ mesenchymal cells migrated to donor RDEB mouse skin and supplemented Col7 in the basement membrane zone. Our previous work showed that embryonic transfer of bone marrow cells into the circulation of RDEB mice resulted in restoration of Col7 via the engraftment of bone marrow–derived

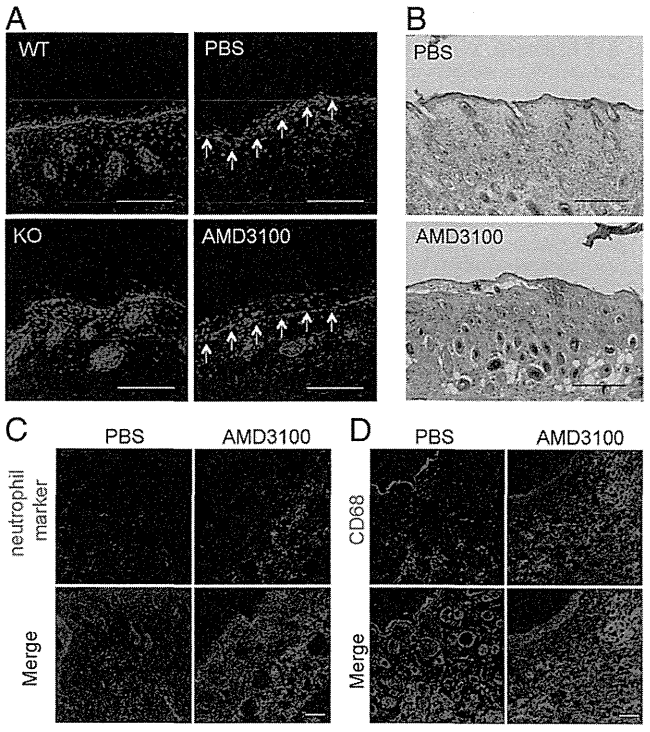

FIGURE 5. Effect of a CXCR4 antagonist on grafted Col7-null mouse skin. (**A**) Immunostaining of Col7-null skin grafted on a wild-type mouse at day 14. Arrows point to the basement membrane region of the dermal–epidermal junction. (**B**) Hematoxylin-eosin staining of grafted Col7-null skin on a wild-type mouse at day 14. Asterisk indicates the blister cavity. (**C**) Immunostaining for neutrophil markers and (**D**) CD68 in Col7-null skin grafted on a wild-type mouse at day 14 with or without AMD3100 treatment. KO, Col7 knockout mouse skin graft (negative control); PBS, PBS-administered Col7 knock-out mouse skin graft, AMD3100, AMD3100-administered Col7 knockout mouse skin graft; WT, wild-type mouse skin graft (positive control). Red, Col7; blue, DAPI. Scale bars, 100 μm.

fibroblasts (1). Col7 is believed to be produced predominantly by epidermal keratinocytes and less so, but still at physiologically relevant levels, by dermal fibroblasts (1, 41–43). Our study suggests that bone marrow MSCs may supplement Col7 in a third-party manner by differentiating into circulating PDGFRα+ mesenchymal cells, which then migrate to the injured skin and differentiate into not only dermal fibroblasts but also epidermal keratinocytes if the epidermis is severely damaged (14). In this context, it is noteworthy that transplanted cultured MSCs were previously shown to supply Col7 to the dermal–epidermal junction of Col7-null mice and Col7-null RDEB patients, thereby preventing blistering (28, 44).

Collectively, our data together with previous reports suggest that bone marrow–derived mesenchymal cells, including PDGFRα+ cells, could be a putative source of Col7 in RDEB patient skin, although the role of PDGFRα+ bone marrow cells in the human setting needs to be investigated further for future clinical applications.

Disclosures

The authors have no financial conflicts of interest.

References

1. Chino, T., K. Tamai, T. Yamazaki, S. Otsuru, Y. Kikuchi, K. Nimura, M. Endo, M. Nagai, J. Uitto, Y. Kitajima, and Y. Kaneda. 2008. Bone marrow cell transfer into fetal circulation can ameliorate genetic skin diseases by providing fibroblasts to the skin and inducing immune tolerance. *Am. J. Pathol.* 173: 803–814.
2. Wagner, J. E., A. Ishida-Yamamoto, J. A. McGrath, M. Hordinsky, D. R. Keene, D. T. Woodley, M. Chen, M. J. Riddle, M. J. Osborn, T. Lund, et al. 2010. Bone marrow transplantation for recessive dystrophic epidermolysis bullosa. *N. Engl. J. Med.* 363: 629–639.
3. Prockop, D. J. 2009. Repair of tissues by adult stem/progenitor cells (MSCs): controversies, myths, and changing paradigms. *Mol. Ther.* 17: 939–946.
4. Orkin, S. H., and L. I. Zon. 2008. Hematopoiesis: an evolving paradigm for stem cell biology. *Cell* 132: 631–644.
5. Pittenger, M. F., A. M. Mackay, S. C. Beck, R. K. Jaiswal, R. Douglas, J. D. Mosca, M. A. Moorman, D. W. Simonetti, S. Craig, and D. R. Marshak. 1999. Multilineage potential of adult human mesenchymal stem cells. *Science* 284: 143–147.
6. Prockop, D. J. 1997. Marrow stromal cells as stem cells for nonhematopoietic tissues. *Science* 276: 71–74.
7. Pereira, R. F., K. W. Halford, M. D. O'Hara, D. B. Leeper, B. P. Sokolov, M. D. Pollard, O. Bagasra, and D. J. Prockop. 1995. Cultured adherent cells from marrow can serve as long-lasting precursor cells for bone, cartilage, and lung in irradiated mice. *Proc. Natl. Acad. Sci. USA* 92: 4857–4861.
8. Galmiche, M. C., V. E. Koteliansky, J. Brière, P. Hervé, and P. Charbord. 1993. Stromal cells from human long-term marrow cultures are mesenchymal cells that differentiate following a vascular smooth muscle differentiation pathway. *Blood* 82: 66–76.
9. Tropel, P., N. Platet, J. C. Platel, D. Noël, M. Albrieux, A. L. Benabid, and F. Berger. 2006. Functional neuronal differentiation of bone marrow-derived mesenchymal stem cells. *Stem Cells* 24: 2868–2876.
10. Kang, S. K., L. A. Putnam, J. Ylostalo, I. R. Popescu, J. Dufour, A. Belousov, and B. A. Bunnell. 2004. Neurogenesis of Rhesus adipose stromal cells. *J. Cell Sci.* 117: 4289–4299.
11. Deng, W., Q. Han, L. Liao, C. Li, W. Ge, Z. Zhao, S. You, H. Deng, F. Murad, and R. C. Zhao. 2005. Engrafted bone marrow-derived flk-(1+) mesenchymal stem cells regenerate skin tissue. *Tissue Eng.* 11: 110–119.
12. Brittan, M., K. M. Braun, L. E. Reynolds, F. J. Conti, A. R. Reynolds, R. Poulsom, M. R. Alison, N. A. Wright, and K. M. Hodivala-Dilke. 2005. Bone marrow cells engraft within the epidermis and proliferate in vivo with no evidence of cell fusion. *J. Pathol.* 205: 1–13.
13. Fathke, C., L. Wilson, J. Hutter, V. Kapoor, A. Smith, A. Hocking, and F. Isik. 2004. Contribution of bone marrow-derived cells to skin: collagen deposition and wound repair. *Stem Cells* 22: 812–822.
14. Tamai, K., T. Yamazaki, T. Chino, M. Ishii, S. Otsuru, Y. Kikuchi, S. Iinuma, K. Saga, K. Nimura, T. Shimbo, et al. 2011. PDGFRalpha-positive cells in bone marrow are mobilized by high mobility group box 1 (HMGB1) to regenerate injured epithelia. *Proc. Natl. Acad. Sci. USA* 108: 6609–6614.
15. Morikawa, S., Y. Mabuchi, Y. Kubota, Y. Nagai, K. Niibe, E. Hiratsu, S. Suzuki, C. Miyauchi-Hara, N. Nagoshi, T. Sunabori, et al. 2009. Prospective identification, isolation, and systemic transplantation of multipotent mesenchymal stem cells in murine bone marrow. *J. Exp. Med.* 206: 2483–2496.
16. Takashima, Y., T. Era, K. Nakao, S. Kondo, M. Kasuga, A. G. Smith, and S. Nishikawa. 2007. Neuroepithelial cells supply an initial transient wave of MSC differentiation. *Cell* 129: 1377–1388.
17. Hocking, A. M., and N. S. Gibran. 2010. Mesenchymal stem cells: paracrine signaling and differentiation during cutaneous wound repair. *Exp. Cell Res.* 316: 2213–2219.
18. Wu, Y., R. C. Zhao, and E. E. Tredget. 2010. Concise review: bone marrow-derived stem/progenitor cells in cutaneous repair and regeneration. *Stem Cells* 28: 905–915.
19. Kuznetsov, S. A., M. H. Mankani, S. Gronthos, K. Satomura, P. Bianco, and P. G. Robey. 2001. Circulating skeletal stem cells. *J. Cell Biol.* 153: 1133–1140.
20. Kuznetsov, S. A., M. H. Mankani, A. I. Leet, N. Ziran, S. Gronthos, and P. G. Robey. 2007. Circulating connective tissue precursors: extreme rarity in humans and chondrogenic potential in guinea pigs. *Stem Cells* 25: 1830–1839.
21. Granero-Moltó, F., J. A. Weis, M. I. Miga, B. Landis, T. J. Myers, L. O'Rear, L. Longobardi, E. D. Jansen, D. P. Mortlock, and A. Spagnoli. 2009. Regenerative effects of transplanted mesenchymal stem cells in fracture healing. *Stem Cells* 27: 1887–1898.
22. Otsuru, S., K. Tamai, T. Yamazaki, H. Yoshikawa, and Y. Kaneda. 2008. Circulating bone marrow-derived osteoblast progenitor cells are recruited to the bone-forming site by the CXCR4/stromal cell-derived factor-1 pathway. *Stem Cells* 26: 223–234.
23. Ceradini, D. J., A. R. Kulkarni, M. J. Callaghan, O. M. Tepper, N. Bastidas, M. E. Kleinman, J. M. Capla, R. D. Galiano, J. P. Levine, and G. C. Gurtner. 2004. Progenitor cell trafficking is regulated by hypoxic gradients through HIF-1 induction of SDF-1. *Nat. Med.* 10: 858–864.
24. Askari, A. T., S. Unzek, Z. B. Popovic, C. K. Goldman, F. Forudi, M. Kiedrowski, A. Rovner, S. G. Ellis, J. D. Thomas, P. E. DiCorleto, et al. 2003. Effect of stromal-cell-derived factor 1 on stem-cell homing and tissue regeneration in ischaemic cardiomyopathy. *Lancet* 362: 697–703.
25. Ma, Q., D. Jones, and T. A. Springer. 1999. The chemokine receptor CXCR4 is required for the retention of B lineage and granulocytic precursors within the bone marrow microenvironment. *Immunity* 10: 463–471.
26. Nagasawa, T., S. Hirota, K. Tachibana, N. Takakura, S. Nishikawa, Y. Kitamura, N. Yoshida, H. Kikutani, and T. Kishimoto. 1996. Defects of B-cell lymphopoiesis and bone-marrow myelopoiesis in mice lacking the CXC chemokine PBSF/SDF-1. *Nature* 382: 635–638.
27. Heinonen, S., M. Männikkö, J. F. Klement, D. Whitaker-Menezes, G. F. Murphy, and J. Uitto. 1999. Targeted inactivation of the type VII collagen gene (Col7a1) in mice results in severe blistering phenotype: a model for recessive dystrophic epidermolysis bullosa. *J. Cell Sci.* 112: 3641–3648.

28. Alexeev, V., J. Uitto, and O. Igoucheva. 2011. Gene expression signatures of mouse bone marrow-derived mesenchymal stem cells in the cutaneous environment and therapeutic implications for blistering skin disorder. *Cytotherapy* 13: 30–45.
29. Morikawa, S., Y. Mabuchi, K. Niibe, S. Suzuki, N. Nagoshi, T. Sunabori, S. Shimmura, Y. Nagai, T. Nakagawa, H. Okano, and Y. Matsuzaki. 2009. Development of mesenchymal stem cells partially originate from the neural crest. *Biochem. Biophys. Res. Commun.* 379: 1114–1119.
30. Sasaki, M., R. Abe, Y. Fujita, S. Ando, D. Inokuma, and H. Shimizu. 2008. Mesenchymal stem cells are recruited into wounded skin and contribute to wound repair by transdifferentiation into multiple skin cell type. *J. Immunol.* 180: 2581–2587.
31. Chen, L., E. E. Tredget, P. Y. Wu, and Y. Wu. 2008. Paracrine factors of mesenchymal stem cells recruit macrophages and endothelial lineage cells and enhance wound healing. *PLoS One* 3: e1886.
32. Wu, Y., J. Wang, P. G. Scott, and E. E. Tredget. 2007. Bone marrow-derived stem cells in wound healing: a review. *Wound Repair Regen.* 15(Suppl 1): S18–S26.
33. Kavanagh, H., and B. P. Mahon. 2011. Allogeneic mesenchymal stem cells prevent allergic airway inflammation by inducing murine regulatory T cells. *Allergy* 66: 523–531.
34. Choi, H., R. H. Lee, N. Bazhanov, J. Y. Oh, and D. J. Prockop. 2011. Anti-inflammatory protein TSG-6 secreted by activated MSCs attenuates zymosan-induced mouse peritonitis by decreasing TLR2/NF-κB signaling in resident macrophages. *Blood* 118: 330–338.
35. Németh, K., A. Leelahavanichkul, P. S. Yuen, B. Mayer, A. Parmelee, K. Doi, P. G. Robey, K. Leelahavanichkul, B. H. Koller, J. M. Brown, et al. 2009. Bone marrow stromal cells attenuate sepsis via prostaglandin E(2)-dependent reprogramming of host macrophages to increase their interleukin-10 production. *Nat. Med.* 15: 42–49.
36. English, K., J. M. Ryan, L. Tobin, M. J. Murphy, F. P. Barry, and B. P. Mahon. 2009. Cell contact, prostaglandin E(2) and transforming growth factor beta 1 play non-redundant roles in human mesenchymal stem cell induction of CD4+ CD25(High) forkhead box P3+ regulatory T cells. *Clin. Exp. Immunol.* 156: 149–160.
37. Ji, J. F., B. P. He, S. T. Dheen, and S. S. Tay. 2004. Interactions of chemokines and chemokine receptors mediate the migration of mesenchymal stem cells to the impaired site in the brain after hypoglossal nerve injury. *Stem Cells* 22: 415–427.
38. Cheng, Z., L. Ou, X. Zhou, F. Li, X. Jia, Y. Zhang, X. Liu, Y. Li, C. A. Ward, L. G. Melo, and D. Kong. 2008. Targeted migration of mesenchymal stem cells modified with CXCR4 gene to infarcted myocardium improves cardiac performance. *Mol. Ther.* 16: 571–579.
39. Sackstein, R., J. S. Merzaban, D. W. Cain, N. M. Dagia, J. A. Spencer, C. P. Lin, and R. Wohlgemuth. 2008. Ex vivo glycan engineering of CD44 programs human multipotent mesenchymal stromal cell trafficking to bone. *Nat. Med.* 14: 181–187.
40. Ip, J. E., Y. Wu, J. Huang, L. Zhang, R. E. Pratt, and V. J. Dzau. 2007. Mesenchymal stem cells use integrin beta1 not CXC chemokine receptor 4 for myocardial migration and engraftment. *Mol. Biol. Cell* 18: 2873–2882.
41. Ryynänen, J., S. Sollberg, M. G. Parente, L. C. Chung, A. M. Christiano, and J. Uitto. 1992. Type VII collagen gene expression by cultured human cells and in fetal skin. Abundant mRNA and protein levels in epidermal keratinocytes. *J. Clin. Invest.* 89: 163–168.
42. Woodley, D. T., R. A. Briggaman, W. R. Gammon, and E. J. O'Keefe. 1985. Epidermolysis bullosa acquisita antigen is synthesized by human keratinocytes cultured in serum-free medium. *Biochem. Biophys. Res. Commun.* 130: 1267–1272.
43. Stanley, J. R., N. Rubinstein, and V. Klaus-Kovtun. 1985. Epidermolysis bullosa acquisita antigen is synthesized by both human keratinocytes and human dermal fibroblasts. *J. Invest. Dermatol.* 85: 542–545.
44. Conget, P., F. Rodriguez, S. Kramer, C. Allers, V. Simon, F. Palisson, S. Gonzalez, and M. J. Yubero. 2010. Replenishment of type VII collagen and re-epithelialization of chronically ulcerated skin after intradermal administration of allogeneic mesenchymal stromal cells in two patients with recessive dystrophic epidermolysis bullosa. *Cytotherapy* 12: 429–431.

STEM CELLS®

TISSUE-SPECIFIC STEM CELLS

Endogenous Mesenchymal Stromal Cells in Bone Marrow Are Required to Preserve Muscle Function in mdx Mice

RYO FUJITA,[a] KATSUTO TAMAI,[b] ERIKO AIKAWA,[b] KEISUKE NIMURA,[a] SAKI ISHINO,[c] YASUSHI KIKUCHI,[b] YASUFUMI KANEDA[a]

Key Words. Mesenchymal stromal cells • Duchenne muscular dystrophy • TNF-α-stimulated gene/protein-6 • TSG-6 • Muscle satellite cells • Bone marrow cells

[a]Division of Gene Therapy Science, [b]Department of Stem Cell Therapy Science, and [c]Center for Medical Research and Education, Graduate School of Medicine, Osaka University, Osaka, Japan

Correspondence: Katsuto Tamai, M.D., Ph.D., Department of Stem Cell Therapy Science, Graduate School of Medicine, Osaka University, 2-2, Yamada-oka, Suita, Osaka 565-0871, Japan. Telephone: 81-6-6879-3901; Fax: 81-6-6879-3909; e-mail: tamai@gts.med.osaka-u.ac.jp; or Yasufumi Kaneda, M.D., Ph.D., Division of Gene Therapy Science, Graduate School of Medicine, Osaka University, 2-2, Yamada-oka, Suita, Osaka 565-0871, Japan. Telephone: 81-6-6879-3901; Fax: 81-6-6879-3909; e-mail: kaneday@gts.med.osak-u.ac.jp

Received July 9, 2014; accepted for publication October 31, 2014; first published online in STEM CELLS *EXPRESS* November 19, 2014.

1066-5099/2014/$30.00/0

http://dx.doi.org/10.1002/stem.1900

ABSTRACT

The physiological role of "endogenous" bone marrow (BM) mesenchymal stromal cells (MSCs) in tissue regeneration is poorly understood. Here, we show the significant contribution of unique endogenous BM-MSC populations to muscle regeneration in Duchenne muscular dystrophy (DMD) mice (mdx). Transplantation of BM cells (BMCs) from 10-week-old mdx into 3–4-week-old mdx mice increased inflammation and fibrosis and reduced muscle function compared with mdx mice that received BMCs from 10-week-old wild-type mice, suggesting that the alteration of BMC populations in mdx mice affects the progression of muscle pathology. Two distinct MSC populations in BM, that is, hematopoietic lineage (Lin)$^-$/ckit$^-$/CD106$^+$/CD44$^+$ and Lin$^-$/ckit$^-$/CD106$^+$/CD44$^-$ cells, were significantly reduced in 10-week-old mdx mice in disease progression. The results of a whole-transcriptome analysis indicated that these two MSC populations have distinct gene expression profiles, indicating that the Lin$^-$/ckit$^-$/CD106$^+$/CD44$^+$ and Lin$^-$/ckit$^-$/CD106$^+$/CD44$^-$ MSC populations are proliferative- and dormant-state populations in BM, respectively. BM-derived Lin$^-$/CD106$^+$/CD44$^+$ MSCs abundantly migrated to damaged muscles and highly expressed tumor necrosis factor-alpha-stimulated gene/protein-6 (TSG-6), an anti-inflammatory protein, in damaged muscles. We also demonstrated that TSG-6 stimulated myoblast proliferation. The injection of Lin$^-$/ckit$^-$/CD106$^+$/CD44$^+$ MSCs into the muscle of mdx mice successfully ameliorated muscle dysfunction by decreasing inflammation and enhancing muscle regeneration through TSG-6-mediated activities. Thus, we propose a novel function of the unique endogenous BM-MSC population, which countered muscle pathology progression in a DMD model. STEM CELLS *2015;33:962–975*

INTRODUCTION

Bone marrow (BM) is a source of hematopoietic stem cells (HSCs) and also contains nonhematopoietic stromal cell populations known as mesenchymal stromal cells (MSCs). Conventionally, MSCs have been defined as colony-forming unit-fibroblasts (CFU-Fs) with the capacity to differentiate into adipocytes, chondrocytes, and osteocytes in vitro [1, 2]. Culture-expanded MSCs have been used to treat various tissue injuries, such as myocardial infarction and lung and skin injuries [3–5]. A focus of great interest regarding the use of culture-expanded MSCs in clinical applications is their anti-inflammatory and regeneration activities, which render the microenvironment more efficient for promoting tissue regeneration [3, 6].

Our previous studies revealed that, similar to culture-expanded BM-MSCs, circulating BM-derived osteoblast progenitor cells were attracted by bone morphogenetic protein-2 to contribute to ectopic bone formation [7, 8]. We also found previously that necrotic skin-derived high-mobility group box 1 (HMGB1) mobilizes platelet-derived growth factor receptor alpha-positive (PDGFRα$^+$) mesenchymal cells from the BM into circulation [9]. These data suggest that injury stimuli attract endogenous BM-MSC populations via the circulation to support tissue regeneration.

However, the characteristics of these endogenous BM-MSC populations mobilized from BM into circulation and damaged tissues have not been established because of their low number and high heterogeneity. In addition, another endogenous function of MSCs in BM is to maintain HSC quality and quantity as a niche by secreting stem cell factor and/or C-X-C type chemokine ligand 12 (CXCL12), known as stromal cell-derived factor 1α (SDF-1α)

[10–14]. Together, the results of our previous investigations along with those of other seminal studies suggest that multiple MSC populations exist in BM, possibly with distinct functions, such as supporting HSCs and contributing to tissue regeneration [15, 16].

Although information regarding the functions and surface markers of culture-expanded MSCs has accumulated, the molecular characteristics of endogenous BM-MSCs are still poorly understood [17, 18]. It is thus necessary to explore BM-MSC populations contributing to the tissue regeneration processes and their molecular signatures —such as gene expression profiles—to elucidate the specific functions of each MSC population in vivo. In previous research, we investigated the dynamics of BM-MSCs in acute injury and regeneration models [8, 9], but it remains unclear whether endogenous BM-MSCs also support tissue regeneration in chronic tissue damage and regeneration processes, such as those in Duchenne muscular dystrophy (DMD).

DMD is characterized primarily by progressive muscle degeneration and weakness due to mutations in the dystrophin gene [19–21]. Muscle cells without dystrophin are vulnerable to damage, resulting in cycles of degeneration and regeneration, chronic inflammation, severe fibrosis, and reduced muscle contractility. Currently, therapies for DMD can be divided into two groups: treatments targeting the restoration of dystrophin expression by cell therapies [22–26] and treatments for tilting the balance of overall muscle condition in favor of regeneration by the activation of satellite cells and the suppression of inflammation and fibrosis [27, 28]. However, there is no curative treatment for DMD at present.

In addition to these therapies, boosting endogenous muscle repair mechanisms is an alternative and feasible approach to treat muscle diseases. In light of the accumulated findings, the activation of muscle repair mechanisms by endogenous BM-MSCs could be an attractive novel approach to slow the progression of muscle dysfunction in DMD. For this purpose, a better understanding of the roles of endogenous BM-MSCs in the pathology of DMD as well as the identification of endogenous molecular characteristics in vivo is urgently required.

In this study, we investigated the contribution of "endogenous" BM-MSCs to muscle regeneration in a DMD mouse model (mdx). Using a bone marrow transplantation (BMT) model, we found that alterations of the endogenous BM-MSC population affect the muscle pathological conditions in mdx mice. In an evaluation of an endogenous BM-MSC population by a whole-genome transcriptome analysis and flow cytometry analysis, we characterized the heterogeneity of endogenous BM-MSCs and identified the dominantly recruited BM-MSC population into damaged muscles in mdx mice. The treatment of this specific BM-MSC population alone stimulated the muscle regeneration processes. We believe that these findings provide new insight into muscle repair mechanisms with specific endogenous BM-MSC populations, and our results contribute to the understanding of BM-MSC-mediated muscle repair mechanisms that can slow disease progression in DMD.

Materials and Methods

Mice

All animals were handled according to approved protocols and the guidelines of the Animal Committee of the Osaka University Graduate School of Medicine. C57BL/6, C57BL/10ScSn/J, and C57BL/10ScSn-Dmd^{mdx}/J (referred to as mdx) mice were purchased from CLEA Japan (Tokyo). C57BL/6 mice that ubiquitously expressed enhanced green fluorescent protein (GFP, referred to as GFP mice) were kindly provided by Masaru Okabe (Osaka University, Osaka, Japan). B6.129S4-Pdgfra$^{tm11(EGFP)Sor}$/J mice (referred to as PDGFRα-H2BGFP) were purchased from The Jackson Laboratory (West Grove, PA). PDGFRα-H2BGFP mice were heterozygous knockin mice in which the histone H2B-GFP fusion gene was inserted into the locus of the PDGFRα gene.

Muscle Endurance Test and Grip-Strength Test

To determine the muscle endurance in mice, a mouse was allowed to grasp the bar or metallic mesh and remain suspended (Supporting Information Fig. S1F, S1G). The time until the mouse released its grip was recorded. Each mouse was subjected to six tests, and the results from these tests were averaged. The final outcome value for the muscle endurance was determined using the holding impulse (second × body weight, g) to correct for the negative effects of body mass on the hang time. The whole-limb grip strength was measured using a Grip Strength Meter for mice (Muromachi Kikai, Tokyo). The mouse was allowed to grasp a horizontal mesh platform with all four limbs, and then, the mouse's tail was pulled back parallel to the mesh platform. The peak tension (gram; g) was recorded when the mouse released its grip. Six sets of measurements were performed for each mouse, and the average values were defined as the mouse whole-limb grip strength.

Isolation of Bone Marrow Cells and Bone Marrow Transplantation

The isolation of BM cells (BMCs) and BMT was performed as described [7, 9]. Briefly, under sterile conditions, BMCs were isolated by flushing the femurs and tibiae with 2% fetal bovine serum (FBS)/phosphate-buffered saline (PBS). For the total BMT, 5×10^6 BMCs were injected into the tail veins of mice irradiated with 10 Gy. Six weeks after reconstitution, the chimerisms were examined, and the results confirmed that more than 90% of the total BMCs were donor-derived cells (Supporting Information Fig. S2A, S2B). For the preparation of each mouse with reduced MSCs in BM, GFP$^+$/Lin$^-$/ckit$^+$ BMCs, which include HSC but not MSC populations, were sorted with the FACSAria II cell sorter (BD Biosciences, San Jose, CA; Supporting Information Fig. S3A). Each irradiated mouse received $1 \times 10^5 - 2 \times 10^5$ GFP$^+$/Lin$^-$/ckit$^+$ BMCs, the number of which was almost identical to that of the GFP$^+$/Lin$^-$/ckit$^+$ BMCs for the total BMT. After reconstitution, the numbers and percentages of donor-derived-MSC populations in BM were examined (Supporting Information Fig. S3B–S3F).

Preparation of Conditioned Media

For the preparation of conditioned media, culture-expanded BM-MSCs at passage 3 were used. The BM-MSCs were stimulated with 10% wild-type (WT) or mdx mouse serum for 2 days. The medium was then changed to fresh α-MEM, and another 2 days of incubation was performed. The conditioned media of these cells were collected and used to stimulate C2C12 cells.

Isolation of Primary Satellite Cells and C2C12 Cells

For the isolation of single myofibers, the extensor digitorum longus muscles were isolated and digested in 0.2% collagenase for 90 minutes at 37°C, as described [29]. Primary myoblasts were obtained from all hind limb muscles, according to the procedure of Musaro and Barberi [30]. C2C12 cells were obtained from the American Type Culture Collection (Rockville, MD). For antibody treatment, C2C12 cells were preincubated for 1 hour with 2.5 μg/ml of control IgG (rat IgG) or blocking antibody for CD44 (clone KM81; Abcam, Cambridge, MA) with or without BM-MSC-derived condition media. Recombinant mouse tumor necrosis factor-alpha (TNF-α)-stimulated gene/protein-6 (TSG-6) (0.5 mg/ml) was applied to stimulate the C2C12 cells for 48 hours.

Colony-Forming Unit Assay

Lin^- BMCs were collected to exclude all hematopoietic lineage cells from total BMCs by the MACS system (Miltenyi Biotec, Bergisch Gladbach, Germany). Isolated Lin^- BMCs were then seeded in a six-well plate. The adherent cells were stained as described [31]. The numbers of colonies containing more than 50 cells were counted under a light microscope.

In Vivo Migration Assay

Silicon tubes containing either PBS or SDF-1α (100 ng/ml; Peprotech, Rocky Hill, NJ) were implanted under the skin of mdx mice. After 2 days, the tubes were collected and cultured for 2 days and analyzed by immunocytochemistry.

Muscle Injury and Treatment

To induce muscle injury, a cardiotoxin (CTX; *Naja mossambica* venom; Sigma, St. Louis, MO) was used [32]. For cell treatment, freshly isolated BMCs (1×10^5) were injected directly into both the superior and inferior regions of CTX-damaged WT or mdx muscles. The day after treatment, 10 μg of CD44 antibody (clone KM81, Abcam) and 5 μg of TSG-6 antibody (clone MAB2104, R&D Systems, Minneapolis, MN) were administered to the muscles. As a control, the same amounts of rat or mouse IgG (R&D Systems) were used. Recombinant mouse TSG-6 (2 μg in 10 μl of PBS; R&D Systems) was administered to the muscles. The same volume of PBS was injected into the muscle as a control.

Histology and Immunostaining

Hematoxylin and eosin (H&E) staining was performed as described [32]. For collagen staining, a picrosirius red staining kit was used (Polysciences, Warrington, PA). The average cross-sectional area (CSA) of muscle fibers was measured using NIH ImageJ software. Only regenerating muscle fibers with central nuclei (100–300 fibers per muscle) were measured. The antibodies used for immunostaining are listed in Supporting Information Table S1. For the nuclear staining, prolong gold antifade reagent containing DAPI (Life Technologies, Carlsbad, CA) was used. The MyoD-, Pax7-, and embryonic myosin heavy chain (eMyHC)-positive cells and the area in three regions of cross-section per mouse were determined by NIH ImageJ software.

Evans Blue Dye Uptake

First, 10 mg/ml of Evans blue dye (EBD) stock solution was prepared in PBS. A single dose (50 mg/g of b.wt.) was administered to the mouse by intraperitoneal injection. The mice were sacrificed 20 hours later, and the muscles were dissected. The EBD^+ cells per muscle were counted in five regions using ×20 magnification sections.

Fluorescence-Activated Cell Sorting Analysis and Sorting of Bone Marrow Cells

Isolated BMCs containing 2×10^6 cells were suspended in 200 μl of staining buffer (2% FBS in PBS), followed by an incubation with purified rat anti-mouse CD16/CD32 (Mouse BD Fc Block, BD Pharmingen, San Diego, CA) for 10 minutes at 4°C. The fluorescence-conjugated antibodies were incubated for 30 minutes at 4°C. The antibodies used in the flow cytometry analysis are listed in Supporting Information Table S1. Fluorescence was measured by the FACSCanto II (BD Biosciences). Gates were defined based on the isotype control staining. The fluorescence-activated cell sorting data were analyzed using FlowJo software ver. 6.3.3 (Tree Star, Ashland, OR).

Muscle Digestion for the Flow Cytometry Analysis

The harvested muscles (soleus, tibialis anterior [TA], gastrocnemius, and plantaris) were minced into small pieces and digested using 0.2% collagenase A (Roche, Mannheim, Germany) for 40 minutes at 37°C with frequent triturating by pipette. The digested muscles were centrifuged at 1,200 rpm for 5 minutes and then further incubated in 0.2% collagenase/dispase (Roche) for 1 hour at 37°C. Following digestion, the cells were filtered using a sequence of 70-μm and 40-μm nylon mesh strainers, followed by centrifugation at 1,500 rpm for 10 minutes. The pellets were then suspended in the staining buffer and stained with specific antibodies, and the BMC populations in damaged muscles were analyzed and isolated by the BD FACSCanto II and BD FACSAria II, respectively.

Western Blot Analysis

Western blot analyses were performed as described [32]. The antibodies used in the Western blot analysis are listed in Supporting Information Table S1. All bands were visualized by Chemi-Lumi One (Nacalai Tesque, Kyoto, Japan) with Image-Quant LAS 4000mini software (GE Healthcare, Buckinghamshire, U.K.). The band density was analyzed using NIH ImageJ software.

RNA Extraction and Real-Time Polymerase Chain Reaction

Total RNA was extracted from muscle and BMCs using ISOGEN (Nippon Gene, Toyama, Japan) according to the manufacturer's instructions. cDNA was synthesized from an equal quantity of total RNA (2 μg for muscle and 500 ng for sorted BMCs) by reverse transcription using the High Capacity RNA-to-cDNA kit (Applied Biosystems, Foster City, CA). A real-time polymerase chain reaction (PCR) was performed with SYBR PremixEX Taq (Takara Bio, Shiga, Japan) using oligonucleotide primers. The sequences of oligonucleotide primers used for the real-time PCR are listed in Supporting Information Table S2. The quantitative data were obtained in triplicate within a single experiment on a 384-well plate based on the standard curve method using CFX manager software (BioRad, Hercules, CA). All data were normalized to GAPDH levels as an internal control.

RNA Sequencing

RNA was extracted from sorted $Lin^-/ckit^-/CD106^+/CD44^+$ and $Lin^-/ckit^-/CD106^+/CD44^-$ BMCs using ISOGEN (Nippon

Gene) according to the manufacturer's instructions. Strand-specific sequencing libraries from two biological replicate RNA samples were prepared according to the Life Technologies protocol, as described [33]. Briefly, digested poly-A-tailed RNA was ligated to the SOLiD Adaptor Mix and then reverse-transcribed using the SOLiD Total RNA-Seq Kit (Life Technologies). Size-selected first-strand cDNA was amplified by SOLiD 5′ PCR primers and barcoded SOLiD 3′ PCR primers (Life Technologies). RNA-seq libraries were sequenced with the 5500xl Genetic Analyzer (Life Technologies). The resulting reads were mapped using Lifescope (Life Technologies) and analyzed using Cufflinks and CummeRbund [34, 35]. The enrichment of gene ontology was calculated by gene ontology tool Database for Annotation, Visualization, and Integrated Discovery [36, 37].

Statistical Analyses

The values are expressed as the mean ± SEM. Statistical analyses were performed with Student's *t* test using the SPSS ver. 10.0 (Japan, Inc., Tokyo). For all statistical tests, significance was accepted at $p < .05$.

Accession Numbers

The accession number of RNA seq data is DRA002440.

Results

WT and mdx Mouse Bone Marrow Transplantations Showed Different Effects on mdx Muscle Pathology

We first examined whether the transplantation of WT BMCs in mdx mice would ameliorate muscle pathology by restoring dystrophin expression. To address this question, we transplanted BMCs derived from either 10-week-old WT mice (or 10-week-old GFP mice) or mdx mice into lethally irradiated 3–4-week-old mdx mice to generate BMT mice (Fig. 1A; Mdx-wt vs. Mdx-mdx, Supporting Information Fig. S4A; Mdx-GFP). To clarify the influence of BMT itself on muscle pathology, we used age-matched non-BMT mdx mice as controls. The body weights and muscle wet weights were not significantly different between the groups during the experimental period (Supporting Information Fig. S1A, S1B).

We did not detect any BM-derived (GFP^+) myofibers in the soleus muscles of the Mdx-GFP mice (Supporting Information Fig. S4A, S4B) or in the cardiotoxin (CTX)-damaged TA muscles (Supporting Information Fig. S4C, S4D), indicating that BM-derived myofibers are negligible, if any, in the mdx mouse after BMT. However, we found significantly increased collagen deposition, which is a marker of fibrosis, in soleus muscles of the Mdx-mdx mice compared with those of Mdx-wt and Mdx (age-matched non-BMT) mice 7 weeks after BMT (Fig. 1B). The aged-matched, non-BMT mdx mice showed less collagen staining compared with the Mdx-wt mice (Fig. 1B), suggesting certain adverse effects of the lethal-dose irradiation in the BMT procedure on muscle pathology in mdx mice.

To obtain quantitative data for fibrosis [27], we measured the levels of fibronectin and MMP13 in soleus muscles 7 weeks after BMT and found that these fibrosis markers were also significantly higher in the Mdx-mdx mice than in Mdx-wt and Mdx mice (Fig. 1C, 1D; Supporting Information Fig. S1C). MMP13 expression is regulated by TNF-α. TNF-α expression tended to be higher in Mdx-mdx mice than in Mdx-wt and Mdx mice (Supporting Information Fig. S1D), suggesting that TNF-α and MMP13 participate, at least in part, in fibrotic deposition.

In contrast, the expression of TNF-α-stimulated gene/protein-6 (TSG-6), which is an anti-inflammatory mediator, was slightly higher in Mdx-wt mice compared with Mdx-mdx mice (Supporting Information Fig. S1E). EBD staining of soleus muscles 7 weeks after BMT showed greatly enhanced necrotic tissue damage in Mdx-mdx mice compared with Mdx-wt and Mdx mice (Fig. 1E, 1F), suggesting increased necrosis by excess inflammation or decreased overall repair mechanisms in Mdx-mdx mice.

We next analyzed the muscle strength and endurance of those BMT mice from 4 to 7 weeks after BMT using grip strength (Fig. 1G) and two different hang wire tests (Supporting Information Fig. S1F, S1G) [28]. Consistent with the deterioration of muscle pathology observed in the Mdx-mdx mice, the muscle functions in Mdx-mdx mice were significantly lower than those of Mdx-wt and Mdx mice (Fig. 1G; Supporting Information Fig. S1F, S1G). These results suggest that mdx-related alterations in BM have significant adverse effects on the progression of muscular degeneration, whereas normal BMT in mdx mice can rescue this mechanism without dystrophin supplementation.

Chronic Muscle Injury in mdx Mice Induced a Reduction of MSC Populations in BM

In the mdx mouse, massive muscle degeneration starts at approximately 3–4 weeks of age, and the degeneration/regeneration cycle continues throughout the lifespan, although muscle degeneration is milder after 12 weeks of age [38]. We thus examined whether the numbers of BM-MSCs in 10-week-old mdx mice were altered as a result of the systemic effect of the chronic muscle degeneration/regeneration cycle. We used a CFU-F assay to determine the total numbers of MSCs in the BM of 10-week-old mdx mice.

Strikingly, the number of BM CFU-Fs in 10-week-old mdx mice was significantly decreased compared with those in the WT mice (Fig. 2A). BM-MSCs have been shown to be highly heterogeneous. We thus investigated the subpopulations of BM-MSCs in 10-week-old mdx mice by conducting flow cytometry analysis. Both CD106 and CD44 have been reported as being expressed in cultured BM mesenchymal "stem" cells [6]. However, a recent report suggests that freshly isolated BM mesenchymal stem cells do not express CD44, and therefore, the expression of CD44 on MSCs in BM remains controversial [18].

Interestingly, in this study, both the $Lin^-/ckit^-/CD106^+/CD44^+$ and $Lin^-/ckit^-/CD106^+/CD44^-$ subpopulations in BM were greatly reduced in 10-week-old mdx mice (Fig. 2B, 2C), but the percentage of the $Lin^+/ckit^-$ population in BM, which includes mature hematopoietic lineage cells [24], was not significantly different between the 10-week-old mdx and WT mice (Supporting Information Fig. S5A). These differences between WT and mdx mice were not observed at 3 weeks of age, before or immediately after the onset of DMD (Supporting Information Fig. S5B–S5F). The results thus suggest that the reduction of these BM subpopulations depends on DMD progression.

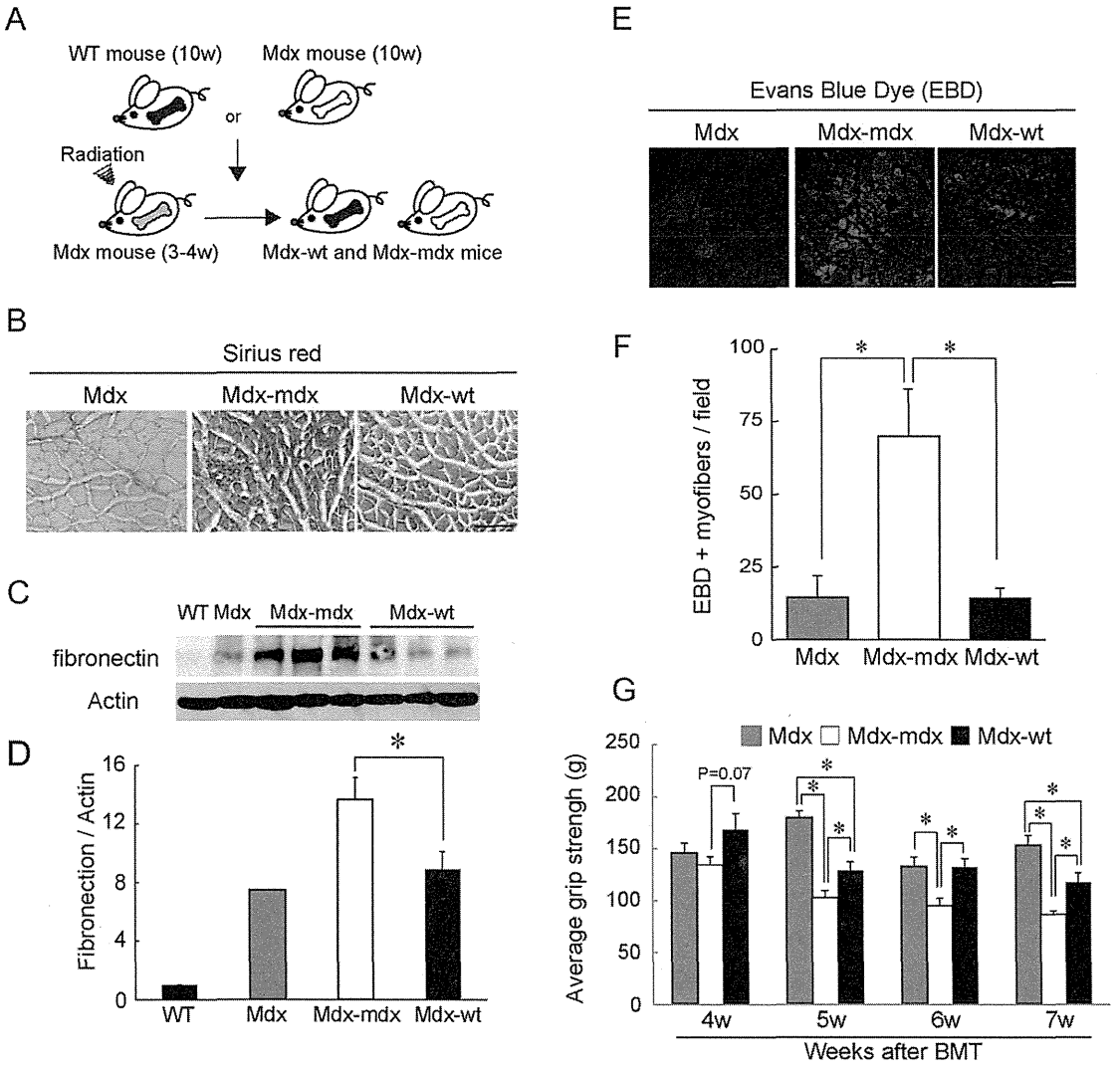

Figure 1. Effects of 10-week-old WT or mdx bone marrow cell (BMC) transplantation on Duchenne muscular dystrophy muscle pathology. **(A):** Schematic illustration of the experimental models. Either 10-week-old WT mouse BMCs or mdx mouse BMCs were transplanted into 3–4-week-old mdx mice after lethal-dose irradiation (Mdx-wt and Mdx-mdx). **(B):** Representative soleus muscle sections of Mdx (age-matched non-BMT control), Mdx-wt, and Mdx-mdx mice stained by picrosirius red 7 weeks after BMT. Scale bar = 200 μm. **(C):** Western blot analyses of fibronectin and Pan-actin (loading control) of soleus muscle 7 weeks after BMT. **(D):** Quantified band densities of fibronectin/actin. The values are the mean ± SEM; *, $p < .05$. **(E):** Representative soleus muscle sections of Mdx (age-matched non-BMT control), Mdx-wt, and Mdx-mdx mice visualized by Evans blue dye (EBD) 7 weeks after BMT. Scale bar = 100 μm. **(F):** The number of EBD^+ fibers was quantified. The values are the mean ± SEM ($n = 4$); *, $p < .05$. **(G):** Measurement of grip strength in Mdx (age-matched non-BMT control), Mdx-wt, and Mdx-mdx mice from 4 to 7 weeks after BMT. The values are the mean ± SEM ($n = 7$–8/group); *, $p < .05$. Abbreviation: BMT, bone marrow transplantation.

To exclude the possibility that these reductions of specific BM subpopulations were simply the result of different degrees of cellularity in dystrophin-deficient BMCs, we established three types of BMT models (Fig. 2D). BMCs from 3-week-old WT mice (donor) were transplanted into either 3-week-old WT (WT-wt) or mdx mice (Mdx-wt) after a lethal dose of irradiation, which replaces the host BMCs with donor BMCs (Supporting Information Fig. S2A, S2B). As another control, BMCs from a 3-week-old mdx mouse (donor), which had BM subpopulations and CFU-F numbers identical to those of WT mice (Supporting Information Fig. S5B–S5F), were transplanted into 3-week-old WT mice (WT-mdx). Both the $Lin^-/ckit^-/CD106^+/CD44^+$ and $Lin^-/ckit^-/CD106^+/CD44^-$ subpopulations in the Mdx-wt mice were significantly lower than those in the WT-wt and WT-mdx mice (Fig. 2E, 2F). These results suggest that both the $Lin^-/ckit^-/CD106^+/CD44^+$ and $Lin^-/ckit^-/CD106^+/CD44^-$ BM subpopulations were gradually reduced by chronic exposure to a muscle injury environment after the onset of muscular dystrophy.

Whole-Transcriptome Analysis of the Reduced MSC Populations in mdx Mice

We further investigated the precise properties of endogenous $Lin^-/ckit^-/CD106^+/CD44^+$ and $Lin^-/ckit^-/CD106^+/CD44^-$ BM populations. PDGFRα has been reported to be expressed in mesenchymal lineage cells [39, 40]. We therefore examined

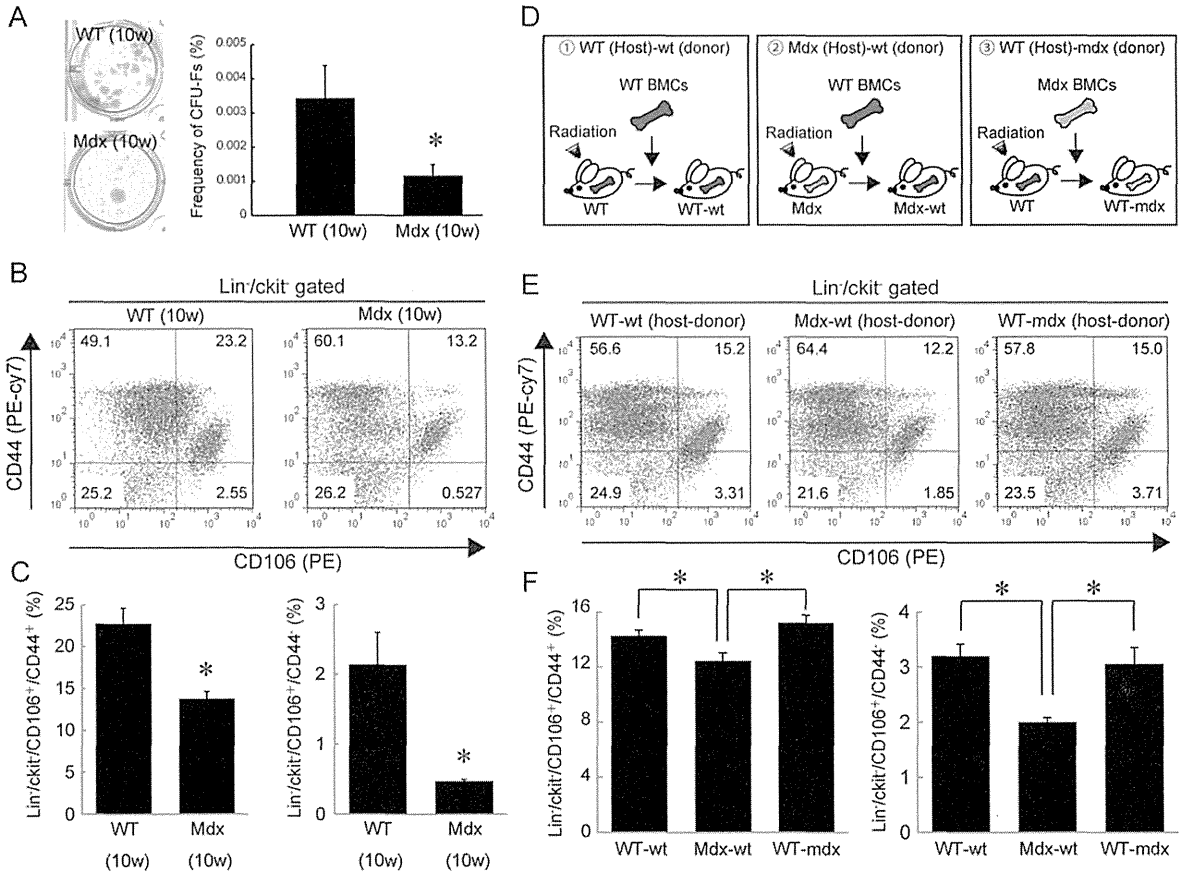

Figure 2. Reduction of mesenchymal stromal cell populations in bone marrow (BM) by chronic muscle injury in mdx mice. **(A):** The numbers of Lin^- cells in the BM of 10-week-old WT and Mdx mice were analyzed in a CFU-F assay. The frequency of CFU-Fs is expressed as the mean ± SEM ($n = 6$/group); *, $p < .05$. **(B):** Representative fluorescence-activated cell sorting (FACS) profiles of BMCs in 10-week-old WT and Mdx mice BM, stained with Lin, ckit, CD106, and CD44. FACS charts gated within $Lin^-/ckit^-$ cells are shown. **(C):** The percentages of $CD106^+/CD44^+$ and $CD106^+/CD44^-$ cells gated within $Lin^-/ckit^-$ cells were quantified. The values are the mean ± SEM ($n = 6$/group); *, $p < .05$. **(D):** Scheme of the bone marrow transplantation (BMT) models, which indicates the following: (1) 3-week-old WT BMCs were transplanted into preirradiated 3-week-old WT mice (WT-wt); (2) 3-week-old WT BMCs were transplanted into preirradiated 3-week-old Mdx mice (Mdx-wt); and (3) 3-week-old Mdx BMCs were transplanted into preirradiated 3-week-old WT mice (WT-mdx). **(E):** Representative FACS profiles of BMCs 7 weeks after BMT, stained with Lin, ckit, CD106, and CD44. FACS plot gated within $Lin^-/ckit^-$ cells is shown. **(F):** The percentages of $CD106^+/CD44^+$ and $CD106^+/CD44^-$ cells gated within $Lin^-/ckit^-$ cells were quantified. The values are the mean ± SEM ($n = 4$/group); *, $p < .05$. Abbreviation: BMC, bone marrow cell.

PDGFRα expression in these BM populations using PDGFRα-H2B GFP mice (see Materials and Methods). $Lin^-/ckit^-/CD106^+/CD44^+$ and $Lin^-/ckit^-/CD106^+/CD44^-$ BM populations comprised 19.9% and 71.9% of the PDGFRα-expressing cells, respectively (Fig. 3A, 3B), suggesting that both of these BM populations contain $PDGFR\alpha^+$ mesenchymal lineage cells.

Next, we conducted a whole-transcriptome analysis by RNA sequencing (RNA seq) analyses to further investigate the molecular properties of these populations. We sorted $Lin^-/ckit^-/CD106^+/CD44^+$ and $Lin^-/ckit^-/CD106^+/CD44^-$ BMCs. The transcript of CD106 mRNA was enriched in the $Lin^-/ckit^-/CD106^+/CD44^+/$ and $Lin^-/ckit^-/CD106^+/CD44^-$ populations, but was not detected in any other populations (Fig. 3C), indicating a successful enrichment of these two populations. Our comparison of the whole-genome transcriptome revealed the enrichment of different functional clusters in each population (Fig. 3D, 3E). The $Lin^-/ckit^-/CD106^+/CD44^+$ population showed significantly higher expression levels of genes, including DNA replication- and cell cycle-related genes (Fig. 3D), such as Myc and Mcm2 (Fig. 3F). In contrast, these genes were not expressed in the $Lin^-/ckit^-/CD106^+/CD44^-$ population. The $Lin^-/ckit^-/CD106^+/CD44^-$ population showed significantly higher expression levels of genes, including cell adhesion- and extracellular matrix receptor interaction-related genes (Fig. 3E). CXCL12 (SDF-1α), Col1A, and FGFR1, which have been reported to be expressed in HSC niche cells [10, 14, 41] (Fig. 3G; Supporting Information Fig. S6).

One of the features associated with stem cell populations is cell-cycle quiescence under physiological conditions. Therefore, to further investigate the differences in the expression of cell cycle-related genes between the two cell populations observed in the RNA seq analysis, we analyzed the expression of the nuclear proliferation marker Ki67 in a flow cytometry analysis. We found that approximately 50% of the $Lin^-/CD106^+/CD44^+$ population was $Ki67^+$, whereas only 10% of the $Lin^-/CD106^+/CD44^-$ population was $Ki67^+$

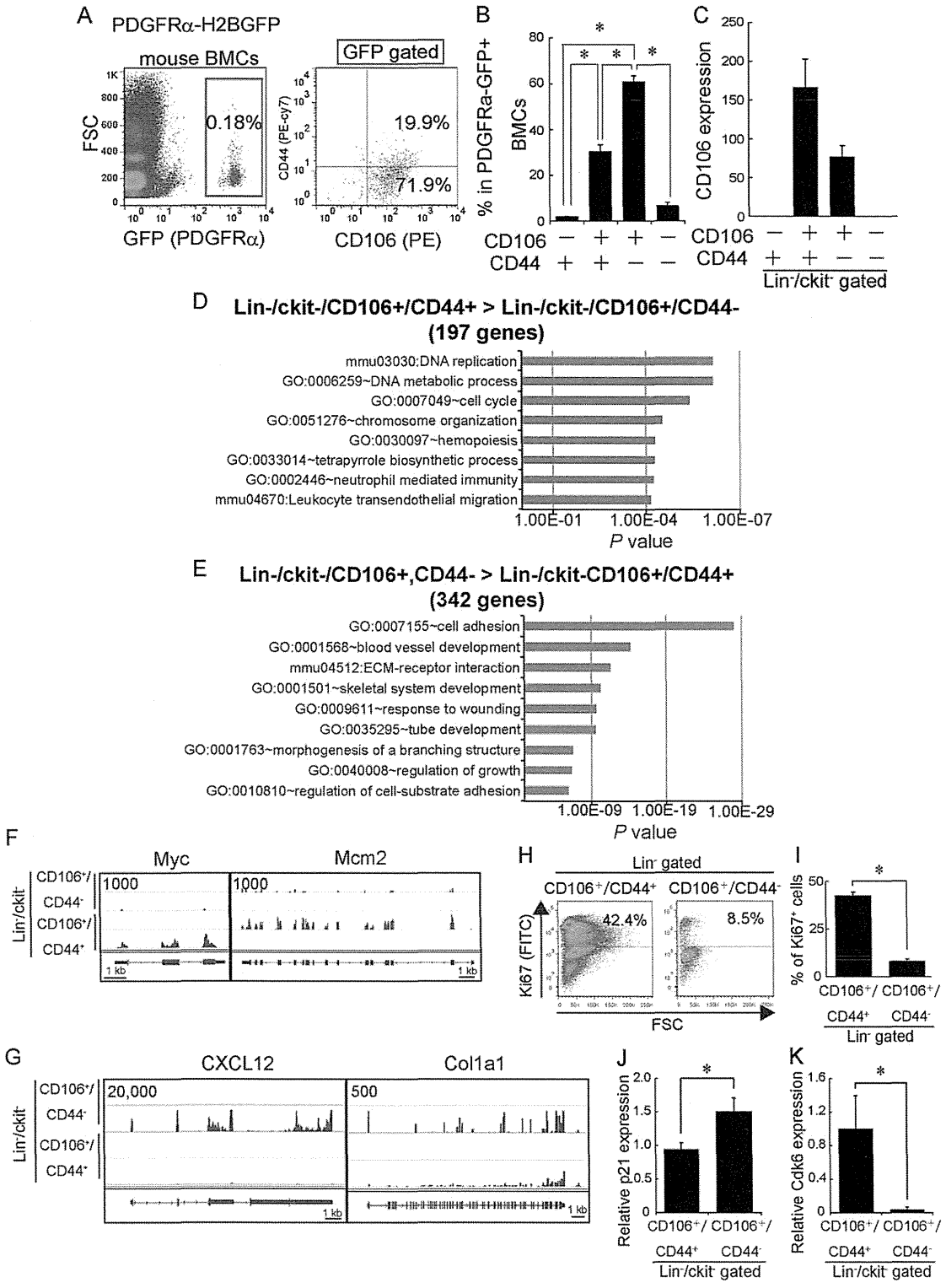

Figure 3. Prospective characterization of freshly isolated mesenchymal stromal cell populations in bone marrow. **(A):** Representative fluorescence-activated cell sorting (FACS) profiles of total BMCs in PDGFRα-H2BGFP knockin mouse. The percentage of PDGFRα-H2BGFP$^+$ cells in total BMCs is shown (left). CD106 and CD44 expression profiles in PDGFRα-GFP$^+$ cells (right). **(B):** The percentages of CD106$^+$/CD44$^+$ and CD106$^+$/CD44$^-$ cells in PDGFRα-GFP$^+$ cells were quantified. The values are the mean ± SEM ($n = 3$/group); *, $p < .05$. **(C):** CD106 mRNA expressions in sorted BMCs. The values are the mean ± SEM. The data are for three independent sorting experiments. **(D, E):** Gene ontology (GO) analysis of RNA seq data from sorted Lin$^-$/ckit$^-$/CD106$^+$/CD44$^+$ and Lin$^-$/ckit$^-$/CD106$^+$/CD44$^-$ BMCs. Genes that are significantly upregulated in Lin$^-$/ckit$^-$/CD106$^+$/CD44$^+$ BMCs (197 genes) or Lin$^-$/ckit$^-$/CD106$^+$/CD44$^+$ cells (342 genes) were categorized by GO annotations. **(F):** RNA-seq results showing the expression of cell cycle-associated genes (Myc and Mcms) in sorted Lin$^-$/ckit$^-$/CD106$^+$/CD44$^+$ and Lin$^-$/ckit$^-$/CD106$^+$/CD44$^-$ BMCs. **(G):** RNA-seq results showing the expressions of CXCL12 (SDF-1α) and Col1a1 in sorted Lin$^-$/ckit$^-$/CD106$^+$/CD44$^+$ and Lin$^-$/ckit$^-$/CD106$^+$/CD44$^-$ BMCs. The RNA-seq data were obtained from two biological replicates. **(H):** Representative FACS profiles of Ki67 expression on Lin$^-$/CD106$^+$/CD44$^+$ and Lin$^-$/CD106$^+$/CD44$^-$ BMCs. **(I):** The percentages of Ki67$^+$ cells on each population were quantified. The values are the mean ± SEM ($n = 3$); *, $p < .05$. **(J, K):** The expressions of cdk6 (J) and p21 (K). The data are for three independent sorting experiments. The values are the mean ± SEM; *, $p < .05$. Abbreviations: BMC, bone marrow cell; FSC, forward scatter; GFP, green fluorescent protein.

(Fig. 3H, 3I). Real-time PCR also revealed that p21, a cell cycle inhibitor gene, showed reduced expression in the $Lin^-/ckit^-/CD106^+/CD44^+$ population than in the $Lin^-/ckit^-/CD106^+/CD44^-$ population (Fig. 3J). In contrast, cyclin-dependent kinase 6 (cdk6) showed higher expression in the $Lin^-/ckit^-/CD106^+/CD44^+$ population than in the $Lin^-/ckit^-/CD106^+/CD44^-$ population (Fig. 3K). Together, these data suggest that $Lin^-/ckit^-/CD106^+/CD44^+$ and $Lin^-/ckit^-/CD106^+/CD44^-$ BM populations, which were decreased in 10-week-old mdx mice, were a proliferative and a slow-dividing mesenchymal lineage, respectively.

Endogenous Migration of BM-Derived MSC Population in Injured Muscles

We then investigated the recruitment of BM-derived mesenchymal populations into damaged muscles. GFP BMCs were transplanted in 3–4-week-old mdx mice (Mdx-GFP), and we analyzed the characteristics of the BM-derived cells recruited to the damaged muscles 4 weeks after BMT by flow cytometry. We found that the Lin^-/GFP^+ cells, which include BM-derived MSC populations (Supporting Information Fig. S7A, S7B), were substantially recruited into the damaged muscle of the mdx mice compared with WT muscles (red squares in Fig. 4A, 4B). Importantly, most of the Lin^-/GFP^+ cells in the damaged muscles expressed both CD106 and CD44 on their surface (red squares in Fig. 4C; Supporting Information Fig. S7C), suggesting that BM-derived $Lin^-/CD106^+/CD44^+$ cells predominantly accumulated into damaged muscle in mdx mice compared with other Lin^-/GFP^+ populations.

These results led us to examine the possible recruitment mechanism of this population. We found that CXCR4 was highly expressed in freshly isolated $Lin^-/ckit^-/CD106^+/CD44^+$ BMCs by the RNA seq (Fig. 4E) and flow cytometry analyses (Supporting Information Fig. S7D). CXCR4 is a receptor for SDF-1α and has been found to be involved in the migration of stem/progenitor cells in various tissues. To elucidate whether the SDF-1α/CXCR4 axis plays a role in recruiting $Lin^-/ckit^-/CD106^+/CD44^+$ BMCs into damaged muscles, we first compared CXCR4 expression in the $Lin^-/ckit^-/CD106^+/CD44^+$ BMCs of WT and mdx mice. We found that CXCR4 expression was slightly but not significantly elevated in the $Lin^-/ckit^-/CD106^+/CD44^+$ BM populations of mdx mice compared with those of the WT mice (Supporting Information Fig. S7E), suggesting that elevated CXCR4 levels are not responsible for the specific migration of $Lin^-/ckit^-/CD106^+/CD44^+$ BMCs into damaged muscles.

Next, we assessed SDF-1α expression in mdx soleus muscles. SDF-1α was specifically detected in mdx muscles but not WT muscles, and $CD68^+$ cells primarily colocalized with SDF-1α signals (Supporting Information Fig. S7F). We also detected significant increases in $Lin^-/ckit^-/CD106^+/CD44^+/CXCR4^+$ cells in the peripheral blood of mdx mice (Fig. 4F). In addition, we implanted silicon tubes containing recombinant SDF-1α under the skin of mdx mice. Two days later, we collected the tubes and counted the numbers and percentages of adherent $CD106^+/CD44^+$ tube-trapped cells. As shown in Supporting Information Figure S7G, S7H, significantly more $CD106^+/CD44^+$ cells migrated into the SDF-1α-containing tubes compared with the tubes containing PBS. These results suggest that the migration of $Lin^-/ckit^-/CD106^+/CD44^+$ BMCs into damaged muscles although the circulation may be partially explained, if not exclusively so, by the CXCR4-SDF-1α pathway.

Function of the BM-Derived MSC Population in Damaged Muscles

Because the TSG-6-mediated immunosuppressive function of cultured expanded MSCs has been documented [42], we next investigated the expression of TSG-6 in the BM-derived $Lin^-/CD106^+/CD44^+$ population in the damaged muscles of Mdx-GFP mice. We found that BM-derived $(GFP^+)/Lin^-/CD106^+/CD44^+$ cells significantly and preferentially expressed TSG-6 in damaged muscles compared with other BM-derived populations (Fig. 5A). However, interleukin-10, which has also been reported to be expressed in BM-MSCs, was not detected (data not shown). It is well known that TSG-6 suppresses inflammation by interacting with CD44 on inflammatory cells, but we also observed the expression of CD44 on the C2C12 myoblasts and primary satellite cells (Fig. 5B; Supporting Information Fig. S8A, S8B). Recombinant TSG-6 (rTSG-6) significantly augmented the proliferation of C2C12 myoblasts (Fig. 5C), suggesting that TSG-6 from BM-MSCs also activated myoblasts.

A previous study suggested that damage signals enhanced TSG-6 expression in BM-MSCs [3], and thus, we investigated whether the treatment of primary BM-MSCs with mdx mouse serum (which contains damage signals) would enhance TSG-6 expression (Fig. 5D). As shown in Figure 5E, elevated TSG-6 expression in mdx serum-treated BM-MSCs was observed, suggesting that the recruited BM-MSC population exposed to damage signals in mdx mice likely elevates TSG-6 expression to suppress inflammation and to activate myoblasts in the damaged muscles.

We also cocultured C2C12 myoblasts with conditioned medium (CM) from BM-MSCs treated with mdx mouse serum for 48 hours (Fig. 5D). We observed a significant proliferation of C2C12 myoblasts following CM treatment (Fig. 5F). However, the CM-mediated C2C12 proliferation was moderately but significantly blocked in the presence of a CD44-neutralizing antibody (Fig. 5F). These data suggest that the TSG-6 secreted from activated BM-MSCs stimulates myoblast activation.

BM-Derived $Lin^-/ckit^-/CD106^+/CD44^+$ Cells Accelerated Muscle Regeneration

Lastly, we examined whether the $Lin^-/ckit^-/CD106^+/CD44^+$ BMCs, the main source of TSG-6 in damaged muscles, could support muscle regeneration. To minimize the effect of the endogenous BM-MSCs population during muscle regeneration, we generated mice with reduced MSCs in BM ($ckit^+$ BMT) by transplanting a sorted $Lin^-/ckit^+$ population (including HSCs but not MSCs) after lethal-dose irradiation (Supporting Information Fig. S3A). As shown in Supporting Information Figure S3B, S3C, the percentage of the $Lin^-/ckit^-$ population in the BM, which includes an MSC population, was significantly less in the $ckit^+$ BMT mice compared with the total BMT mice after 6 weeks of reconstitution. Furthermore, fewer donor BM-derived fibroblastic cells were observed in the $ckit^+$ BMT mice compared with the total BMT mice (Supporting Information Fig. S3D–S3F). These data indicate that $ckit^+$ BMT mice have few endogenous MSCs in their BM.

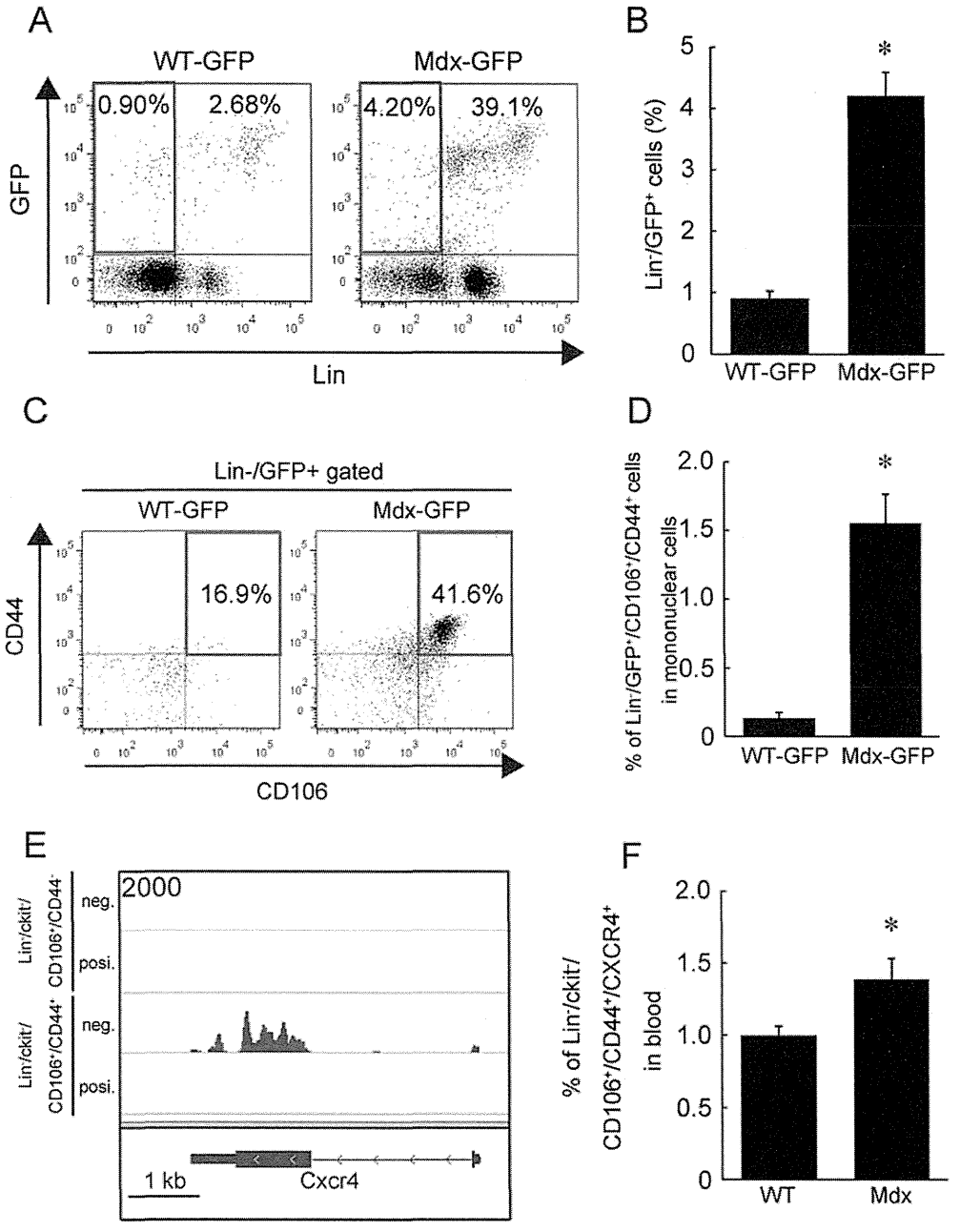

Figure 4. Identification of bone marrow (BM)-mesenchymal stromal cell populations in mdx muscles. **(A):** Flow cytometry analysis in muscles of WT-GFP (left) and Mdx-GFP (right) bone marrow transplantation (BMT) mice performed 4 weeks after BMT. The red squares indicate Lin^-/GFP^+ cells (BM-derived nonhematopoietic cells). **(B):** The percentages of Lin^-/GFP^+ cells were quantified. The values are the mean ± SEM ($n = 4$); *, $p < .05$. **(C):** CD106 and CD44 expression in Lin^-/GFP^+ cells in the muscles of Mdx-GFP BMT mice. Most of the Lin^-/GFP^+ cells were positive for both CD106 and CD44 (red squares). The percentages of $CD106^+/CD44^+$ cells in Lin^-/GFP^+ cells in mdx muscles are shown with red squares. **(D):** The percentages of $Lin^-/GFP^+/CD106^+/CD44^+$ cells in mdx muscles were evaluated. The values are the mean ± SEM ($n = 4$); *, $p < .05$. **(E):** CXCR4 expression from the RNA seq analysis of sorted $Lin^-/ckit^-/CD106^+/CD44^+$ and $Lin^-/ckit^-/CD106^+/CD44^-$ bone marrow cells. **(F):** The percentages of $Lin^-/ckit^-/CD106^+/CD44^+/CXCR4^+$ cells in the peripheral blood of WT and mdx mice were quantified by flow cytometry. The values are the mean ± SEM ($n = 6$–8); *, $p < .05$. Abbreviation: GFP, green fluorescent protein.

Using the $ckit^+$ BMT model, we investigated whether an intramuscular injection of $Lin^-/ckit^-/CD106^+/CD44^+$ BMCs would enhance muscle regeneration in CTX-induced damaged muscles of WT-$ckit^+$ BMT mice (Supporting Information Fig. S9). At 14 days post-treatment, H&E staining showed well-arranged myofibers with fewer mononuclear cells in damaged muscles treated with $Lin^-/ckit^-/CD106^+/CD44^+$ BMCs compared with PBS-treated or $Lin^-/ckit^-/CD106^-/CD44^+$ BMCs-treated damaged muscles, which were the second-most recruited BMCs into damaged muscles (Supporting Information Fig. S9A).

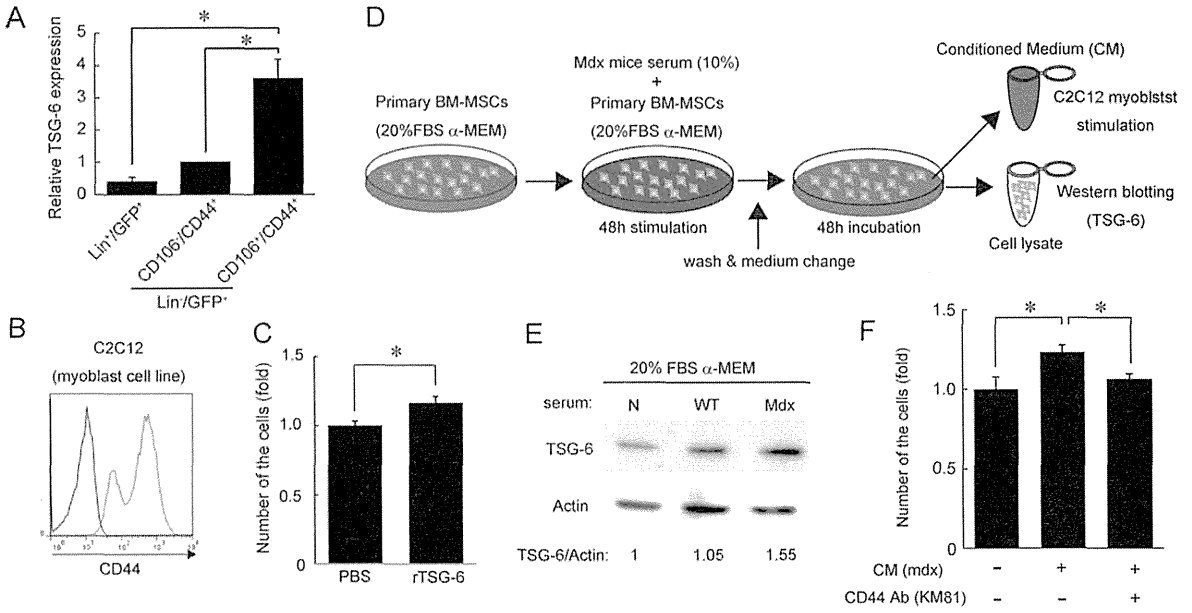

Figure 5. Effect of TSG-6 secreted from BM-MSC populations on myoblasts. **(A):** TSG-6 expression in sorted BM-derived cells from mdx muscles. The values are the mean ± SEM. The data are for three independent sorting experiments; *, $p < .05$. **(B):** Representative fluorescence-activated cell sorting profiles of CD44 expression on C2C12 myoblasts (red line). Isotype control staining is represented by the black line. **(C):** The number of C2C12 myoblasts treated with TSG-6 after 48 hours. **(D):** Strategy for the preparation of CM from primary BM-MSCs. **(E):** Western blot analyses of TSG-6 and Pan-actin (loading control) expression in primary BM-MSCs prepared as in panel (D). **(F):** The number of C2C12 myoblasts treated with CM containing either control IgG (rat IgG) or CD44-blocking antibody (KM81) for 48 hours. The values are the mean ± SEM ($n = 3$); *, $p < .05$. Abbreviations: BM-MSCs, bone marrow-mesenchymal stromal cells; CM, conditioned medium; FBS, fetal bovine serum; PBS, phosphate-buffered saline.

We quantified newly regenerating myofibers or myotubes by counting the desmin$^+$ cells with central nuclei, and the results indicated that the Lin$^-$/ckit$^-$/CD106$^+$/CD44$^+$ BMCs significantly increased the number of desmin$^+$ cells with central nuclei compared with the number in PBS-treated damaged muscles (Supporting Information Fig. S9B, S9C). We also investigated eMyHC$^+$ cell areas in damaged muscle sections. The percentage area of the eMyHC$^+$ cell area was increased by Lin$^-$/ckit$^-$/CD106$^+$/CD44$^+$ BMC treatment compared with PBS- or Lin$^-$/ckit$^-$/CD106$^-$/CD44$^+$ BMC-treated damaged muscle (Supporting Information Fig. S9D, S9E). These data suggest that Lin$^-$/ckit$^-$/CD106$^+$/CD44$^+$ BMCs accelerate muscle regeneration processes in CTX-induced muscle damage.

We next investigated whether Lin$^-$/ckit$^-$/CD106$^+$/CD44$^+$ BMC treatment supports muscle regeneration in Mdx mice. Using Mdx-ckit$^+$ BMT mice reconstituted for 6 weeks (10-week-old mice), we first assessed the effect of Lin$^-$/ckit$^-$/CD106$^+$/CD44$^+$ BMC treatment on satellite cell activation 7 days after cell injection. The injection of Lin$^-$/ckit$^-$/CD106$^+$/CD44$^+$ BMCs increased the number of activated satellite cells, as indicated by MyoD staining (Fig. 6A, 6B). We also observed slightly elevated MyoD expression after Lin$^-$/ckit$^-$/CD106$^+$/CD44$^+$ BMC treatment by Western blotting (Fig. 6C). However, the elevation of the number of MyoD$^+$ satellite cells was partially inhibited by the administration of a CD44-neutralizing antibody or a TSG-6 antibody (Fig. 6A, 6B). MyoD expression also tended to be decreased by the CD44-neutralizing antibody or TSG-6 antibody (Fig. 6C). The number of Pax7$^+$ cells and the expression level of Pax7, which is a quiescent satellite cell marker, were not significantly changed by Lin$^-$/ckit$^-$/CD106$^+$/CD44$^+$ BMC treatment (Supporting Information Fig. S10A–S10C).

We also observed that Lin$^-$/ckit$^-$/CD106$^+$/CD44$^+$ BMC treatment suppressed the infiltration of inflammatory cells and enhanced the overall muscle repair mechanisms in Mdx-ckit$^+$ BMT mice, as assessed by the average muscle fiber CSA at day 7 post-treatment (Fig. 6D, 6E). However, again, the effects of Lin$^-$/ckit$^-$/CD106$^+$/CD44$^+$ BMC treatment on muscle regeneration were partially blocked by a CD44-neutralizing antibody or a TSG-6 antibody (Fig. 6D, 6E). Of note, recombinant TSG-6 treatment also enhanced muscle regeneration with Lin$^-$/ckit$^-$/CD106$^-$/CD44$^+$ BMC treatment (Fig. 6D, 6E). These data may indicate that the BM-derived Lin$^-$/ckit$^-$/CD106$^+$/CD44$^+$ population slowed muscle disease progression by the activation of satellite cells and the suppression of inflammation to enhance the overall repair mechanisms, in part via the TSG-6/CD44-mediated pathway.

Discussion

In this study, we demonstrated for the first time that injured muscular tissues in DMD mice recruit a Lin$^-$/ckit$^-$/CD106$^+$/CD44$^+$ mesenchymal population from the BM to suppress inflammatory and fibrotic reactions and activate a muscular regeneration mechanism. Such chronic injury/regeneration cycles in DMD mice were shown to eventually decrease the MSC populations in BM, resulting in a disruption of the intrinsic anti-inflammatory and regeneration-promoting activities of BM-MSCs to exacerbate muscular dystrophy (Fig. 7).

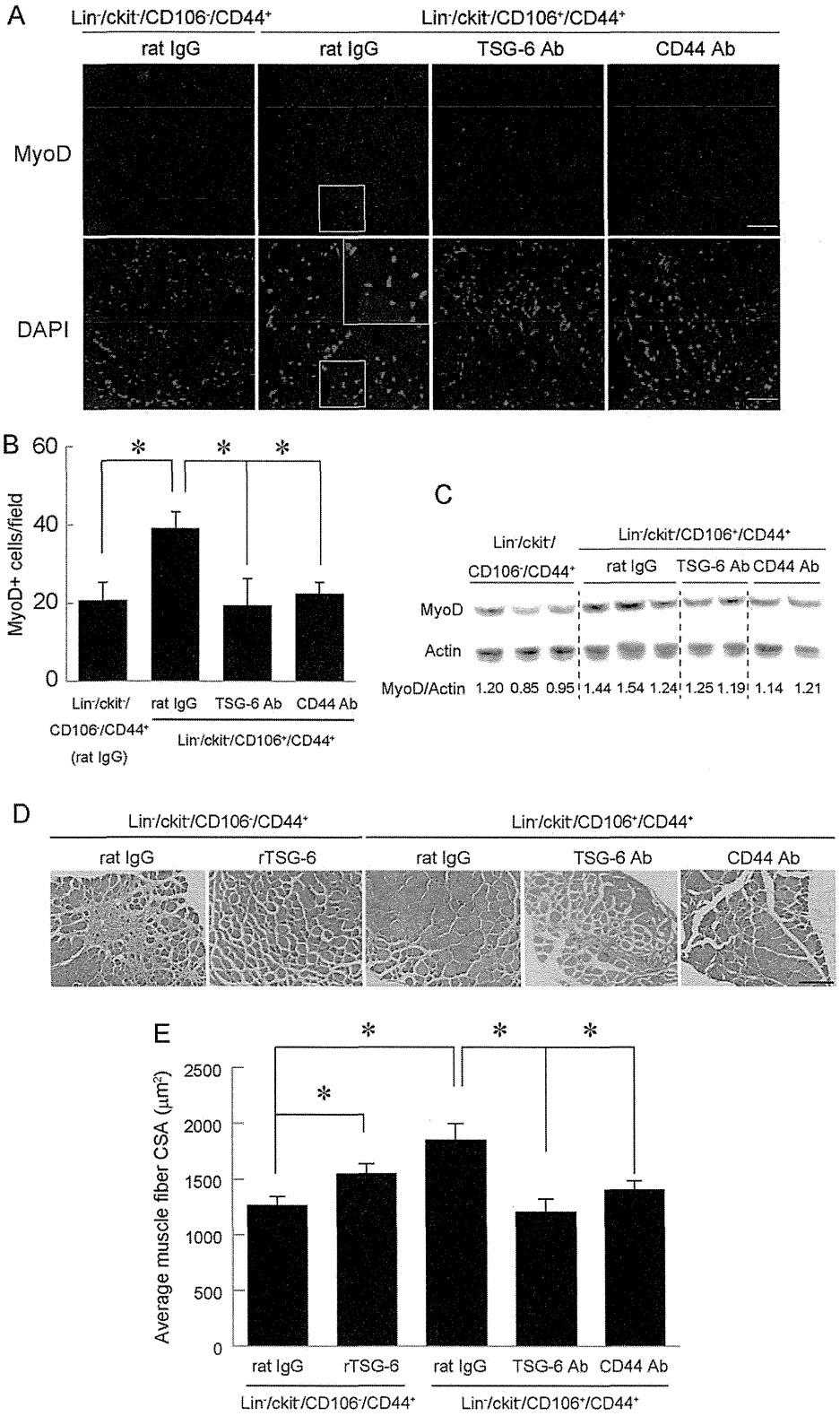

Figure 6. Effect of specific bone marrow-mesenchymal stromal cell populations on skeletal muscle regeneration. **(A):** Immunofluorescent staining for MyoD (red) on tibialis anterior (TA) muscle of Mdx-ckit$^+$ BMT mice 7 days post-treatment of Lin$^-$/ckit$^-$/CD106$^-$/CD44$^+$ or Lin$^-$/ckit$^-$/CD106$^+$/CD44$^+$ bone marrow cells (BMCs) in combination with either a CD44 antibody (KM81) or a TSG-6 antibody. Nuclei were stained with DAPI (blue). Scale bars = 50 μm. **(B):** MyoD$^+$ cells were quantified. The values are the mean ± SEM (n = 3–4/group); *, $p < .05$. **(C):** Western blot analyses of MyoD and Pan-actin (loading control) of TA muscles of Mdx-ckit$^+$ BMT mice at 7 days post-treatment of Lin$^-$/ckit$^-$/CD106$^-$/CD44$^+$ or Lin$^-$/ckit$^-$/CD106$^+$/CD44$^+$ BMCs in combination with either a CD44 antibody (KM81) or a TSG-6 antibody. Quantified band densities of MyoD normalized to actin are also shown. **(D):** H&E staining on TA muscle of Mdx-ckit$^+$ BMT mice 7 days post-treatment of Lin$^-$/ckit$^-$/CD106$^-$/CD44$^+$ or Lin$^-$/ckit$^-$/CD106$^+$/CD44$^+$ BMCs in combination with either recombinant TSG-6 or CD44 antibody (KM81) or TSG-6 antibody. Scale bar = 200 μm. **(E):** The average CSA of muscle fibers with central nuclei was quantified. The values are the mean ± SEM (n = 4–8/group); *, $p < .05$. Abbreviation: CSA, cross-sectional area.